

Dear Editor:

Thank you very much for providing the opportunity for us to revise our paper.

Thank you very much for your contributions to this paper. And we are all extremely grateful for having a chance to make further improvements. The major and minor suggestions of reviewer2# are very helpful for us. Reading and considering all comments of reviewer2# carefully, we have made some revisions on our paper.

Finally, we write the point-by-point response to answer the reviewer2#'s questions for better communication. If there are still any problems on the method, diction, phrasing, grammar, and spelling, please do not hesitate to tell us and we'll try our best to improve them.

Thank you again for your comments to improve our paper. Wish your journal better and better.

Yours,

Mei Hong

2018-03-18

带格式的: 左侧: 3.17 厘米, 右侧: 3.17 厘米, 指定行和字符网格

Responses to reviewer#2:

All the authors are extremely grateful to you for providing your excellent comments and valuable advices for this paper. Your six major suggestions are very helpful for us. Based on your suggestions, we have made some revisions on our paper. We have streamlined the discussion and explained Why p value was in the range 5 to 15 based on your specific comments.

Thank you again for your valuable comments to improve our submission. If there are still any problems on the method, diction, phrasing, grammar, and spelling, please do not hesitate to tell us and we'll try our best to improve them.

In the following, kind comments you suggested before are in black text with corresponding actions taken by us following in blue.

Major comments:

1. Line633-663: I think there is no need to spend space here to introduce the definition of overfitting and you just have to give a reference. The discussion whether the model is overfitting or not is redundant and the discussion should focus on the good forecast results of new examples. This part of the discussion can be properly streamlined.

Responses: Good suggestions. In the previous paper, the discussion whether the model is overfitting or not is redundant and now the discussion have focused on the

good forecast results of new examples. We have deleted some redundant statements to make this part of the discussion can be concise.

The specific revision can be seen from line632 to line647 in page30-31.

We sincerely hope for your satisfaction with our revision. Thank you again for your kind suggestion.

2. Line371: Why p value was in the range 5 to 15? Is this the experience of the predecessors? Or is it the result of the author's own experiment?

Responses: Good suggestions. In the reference (Cao, 1993), if the system forgets slowly, parameters and will be small and the value should be high. And he made a lot of experiments to prove that the p value was in the range 5 to 15 to this system. So the conclusion of p value was in the range 5 to 15 is based on the experience of the predecessors (Cao, 1993). Now we added the explanation of why p value was in the range 5 to 15 for readers' better understanding.

The specific revision can be seen from line370 in page18.

We sincerely hope for your satisfaction with our revision. Thank you again for your kind suggestion.

3. Line597-615: The purpose of this section is to show that a certain impact on the pattern of the 2nd EOF will not make our forecast unstable. But this section here occupied the space too much and I think there is no need to make a list of table5 alone. The author just says the difference among forecast results of both TC and

MAPE of five different sample data are less. Because the main purpose of this paper is to prove that the prediction accuracy of SST and ENSO of the model. Therefore, it is not necessary for table5 to list separately. It is recommended that this part should be simplified.

Responses: Good suggestions. Based on your suggestion, we have deleted the table5 and make the discussion concise. This part had be simplified.

The specific revision can be seen from line596-609 in page29.

We sincerely hope for your satisfaction with our revision. Thank you again for your kind suggestion.

4. Line243-249: The author introduced the standardization of the data before modelling and it is too wordy here. The author just list the standardized formula here. So the section should be suggested to be simplified.

Responses: Good suggestions. Now we have just listed the standardized formula and deleted the redundant statements. So now the section has been simplified.

The specific revision can be seen from line240-246 in page11-12.

We sincerely hope for your satisfaction with our revision. Thank you again for your kind suggestion.

5. Line269 and 298: The abbreviation appears for the first time, and there is no need to repeat the Pearson correlation coefficient (CC).

Responses: Good suggestions. Now we have revised the Pearson correlation coefficient (CC) as CC and the mean absolute percentage error (MAPE) as MAPE in line294 on page14.

We sincerely hope for your satisfaction with our revision. Thank you again for your kind suggestion.

6. Dynamic model recommendations are consistent, the topic is dynamical-st, followed by several dynamic text in a number of tense inconsistency, it is recommended to be consistent.

Responses: Good suggestions. Now we have revised all the “dynamic” as the “dynamical” for the consistency.

The specific revision can be seen in the whole paper.

We sincerely hope for your satisfaction with our revision. Thank you again for your kind suggestion.

Minor comments:

1. Line649: “the forecast results of the Cross-validated” should be revised as” the forecast results of the cross-validated”.

Responses: Good suggestions. Now we have revised “the forecast results of the Cross-validated” as “ the forecast results of the cross-validated” in line631 in page30.

We sincerely hope for your satisfaction with our revision. Thank you again for your kind suggestion.

2. Line 30, “dynamical reconstruction” is more appropriate

Responses : Good suggestions. Now we have revised as “dynamical reconstruction” in line30 on page2.

We sincerely hope for your satisfaction with our revision. Thank you again for your kind suggestion.

3. Line 35, ”pearson” should be ‘’Pearson”

Responses: Good suggestions. Now we have revised “pearson” as “Pearson” in line35 on page2.

We sincerely hope for your satisfaction with our revision. Thank you again for your kind suggestion.

4. Line 36, “approximately” should be ‘’approximate” or “about”

Responses: Good suggestions. Now we have revised “approximately” as “approximate” in line36 on page2.

We sincerely hope for your satisfaction with our revision. Thank you again for your kind suggestion.

5. Line 38, ”but” should be “but also”

Responses: Good suggestions. Now we have revised “but” as “but also” in

line38 on page2.

We sincerely hope for your satisfaction with our revision. Thank you again for your kind suggestion.

6. Line 52,"influences" should be "influence"

Responses : Good suggestions. Now we have revised "influences" as "influence" in line51 on page3.

We sincerely hope for your satisfaction with our revision. Thank you again for your kind suggestion.

7. Line 57,"gradually improved" should be "gradual improvement"

Responses: Good suggestions. Now we have revised "gradually improved" as "gradual improvement" in line56 on page3.

We sincerely hope for your satisfaction with our revision. Thank you again for your kind suggestion.

8. Line 67,"large a amount of" should be " a large amount of "

Responses:Good suggestions. Now we have revised "large a amount of" as "a large amount of" in line66 on page3.

We sincerely hope for your satisfaction with our revision. Thank you again for your kind suggestion.

9. Line 75,"advanced" should be " been advanced "

Responses: Good suggestions. Now we have revised“advanced” as “been advanced” in line74 on page4.

We sincerely hope for your satisfaction with our revision. Thank you again for your kind suggestion.

10. Line 91,”This is because” should be “It is because that”

Responses: Good suggestions. Now we have revised“This is because” as “It is because that” in line90 on page4.

We sincerely hope for your satisfaction with our revision. Thank you again for your kind suggestion.



The following is the a marked-up manuscript version:

带格式的：缩进：首行缩进： 0 厘米

1 **Forecasting experiments of a dynamical-statistical model**
2 **of the sea surface temperature anomaly field based on the**
3 **improved self-memorization principle**

4 Mei Hong^{1,2}, Xi Chen¹, Ren Zhang^{1,2}, Dong Wang³, Shuanghe Shen² and Vijay
5 P. Singh⁴

6 ¹ *Institute of Meteorology and Oceanography, National University of Defense Technology, Nanjing 211101, China*

7 ² *Collaborative Innovation Center on Forecast and Evaluation of Meteorological Disaster, Nanjing University of*
8 *Information Science & Technology, Nanjing 210044, China*

9 ³ *Key Laboratory of Surficial Geochemistry, Ministry of Education; Department of Hydrosiences, School of Earth*
10 *Sciences and Engineering, Collaborative Innovation Center of South China Sea Studies, State Key Laboratory of*
11 *Pollution Control and Resource Reuse, Nanjing University, Nanjing 210093, China*

12 ⁴ *Department of Biological and Agricultural Engineering, Zachry Department of Civil Engineering, Texas A & M*
13 *University, College Station, TX 77843, USA*

14
15
16 Corresponding authors address:

17 1. Xi Chen, Research Centre of Ocean Environment Numerical Simulation, Institute
18 of Meteorology and Oceanography, National University of Defense Technology,
19 Nanjing 211101, China

20 E-mail: chenxigfkd@163.com

21 2. Ren Zhang, Research Centre of Ocean Environment Numerical Simulation,
22 Institute of Meteorology and Oceanography, National University of Defense
23 Technology, Nanjing 211101, China

24 E-mail: 254247175@qq.com

25

26 **Abstract:** With the objective of tackling the problem of inaccurate long-term El Niño
27 Southern Oscillation (ENSO) forecasts, this paper develops a new
28 dynamical-statistical forecast model of sea surface temperature anomaly (SSTA) field.
29 To avoid single initial prediction values, a self-memorization principle is introduced
30 to improve the ~~dynamic~~dynamical reconstruction model, thus making the model more
31 appropriate for describing such chaotic systems as ENSO events. The improved
32 dynamical-statistical model of the SSTA field is used to predict SSTA in the
33 equatorial eastern Pacific and during El Niño and La Niña events. The long-term
34 step-by-step forecast results and cross-validated retroactive hindcast results of time
35 series T_1 and T_2 are found to be satisfactory, with a ~~pearson~~Pearson correlation
36 coefficient of approximately 0.80 and a mean absolute percentage error (MAPE) of
37 less than 15%. The corresponding forecast SSTA field is accurate in that not only is
38 the forecast shape similar to the actual field, but also the contour lines are essentially
39 the same. This model can also be used to forecast the ENSO index. The temporal
40 correlation coefficient is 0.8062, and the MAPE value of 19.55% is small. The
41 difference between forecast results in spring and those in autumn is not high,
42 indicating that the improved model can overcome the spring predictability barrier to
43 some extent. Compared with six mature models published previously, the present
44 model has an advantage in prediction precision and length, and is a novel exploration
45 of the ENSO forecast method.

46 **Keywords:** Dynamical-statistical forecast model; self-memorization principle; sea
47 surface temperature field; long-term forecast of ENSO

48 1. Introduction

49 The El Niño Southern Oscillation (ENSO), the well-known coupled atmosphere
50 –ocean phenomenon, was firstly proposed by Bjerknes (1969). The ENSO
51 phenomenon can influences regional and global climates, so the prediction of ENSO
52 has received considerable public interest (Rasmusson and Carpenter, 1982; Glantz et
53 al., 1991).

54 Over the past two to three decades, one might reasonably expect the ability to
55 predict warm and cold episodes of ENSO at short and intermediate lead times to have
56 ~~gradual improvement~~gradually improved (Barnston et al., 2012). Many countries have
57 been focusing on ENSO forecasts since the 1990s, and the ENSO forecast has become
58 one of the important research topics in the International Climate Change and
59 Predictability Research plan. The U.S. International Research Institute for Climate
60 and Society, the U.S. Climate Prediction Centre, Japan Meteorological Agency, and
61 European Centre for Medium-Range Weather Forecasting have developed different
62 coupled atmosphere–ocean models to forecast ENSO (Saha et al., 2006; Molteni et al.,
63 2007, Zheng et al., 2016) .

64 The forecast models can generally be divided into two types (Palmer et al., 2004,
65 Zheng et al., 2017). The first type is typified by a ~~dynamic~~dynamical model, which
66 mathematically expresses physical laws that govern how the ocean and the
67 atmosphere interact. The second type is typified by a statistical model, which requires
68 a large amount of ~~large a amount of~~ historical data and analyses the data to do
69 forecasting (Chen et al., 1995; Moore et al., 2006).

70 Over the past three decades, ENSO predictions have made remarkable progress,
71 reaching a stage where reasonable statistical and numerical forecasts (Jin et al.,
72 2008) can be made 6–12 months in advance (Wang et al., 2009a). . However, there are
73 three problems remaining to be resolved (Zhang et al., 2003a): (1) The current ENSO
74 predictions are mainly limited to the short term, such as annual and seasonal
75 predictions; (2) Although the representation of ENSO in coupled models has been
76 ~~advanced~~advanced considerably during the last decade, several aspects of the
77 simulated climatology and ENSO are not well reproduced by the current generation of
78 coupled models. The systematic errors in SST are often very large in the equatorial
79 Pacific, and model representations of ENSO variability are often weak and/or
80 incorrectly located (Neelin et al. 1992; Mechoso et al. 1995; Delecluse et al. 1998;
81 Davey et al. 2002). (3) Coupled models of ENSO predictions initialized from
82 observed initial states tend to adjust towards their own climatological mean and
83 variability, leading to forecast errors. The errors associated with such adjustments
84 tend to be more pronounced during boreal spring, which is often called the “spring
85 predictability barrier” (Webster et al., 1999). More efficient models are therefore
86 desired (Belkin and Niyogi, 2003; Weinberger and Saul, 2006). Therefore, the idea of
87 combining dynamical and statistical methods to improve weather and climate
88 prediction has been developed in many studies (Huang et al., 1993; Yu et al., 2014a;
89 Yu et al., 2014b). By introducing genetic algorithms (GAs), Zhang et al. (2006)
90 inverted and reconstructed a new dynamical-statistical forecast model of the tropical
91 Pacific sea surface temperature (SST) field using historic statistical data (Zhang et al.,

92 2008). However, there is one flaw in the forecast model: the time-delayed SST field.
93 ~~It is because that~~~~This is because~~ ENSO is a complicated system with many
94 influencing factors. To overcome information insufficiency in the forecast model,
95 Hong et al. (2014) selected the tropical Pacific SST, SSW and SLP fields as three
96 modelling factors and utilized the GA to optimize model parameters.

97 However, the above dynamical prediction equations which were proposed by
98 Hong et al.(2014), greatly depend on a single initial value, creating long-term
99 forecasts over 8 months that diverged significantly. These unsatisfactory results
100 indicate that this model needs to be improved. Cao (1993) first proposed the
101 self-memorization principle, which transforms the dynamical equations with the
102 self-memorization equations, wherein the observation data can determine the memory
103 coefficients. This method has been widely used in forecast problems in environmental,
104 hydrological and meteorological fields (Feng et al., 2001; Gu, 1998; Chen et al.,
105 2009). The method can avoid the question of initial conditions for the differential
106 equations, so it can be introduced here to improve the proposed dynamical forecast
107 model.

108 Therefore, an improved dynamical-statistical forecast model of the SST field
109 and its impact factors with a self-memorization function was developed. The
110 improved model can absorb the information from past observations.

111 This paper is organized as follows: Research data and forecast factors are
112 introduced in section 2. In Section 3 the reconstruction of the dynamical model of
113 SSTA field is described. To improve the reconstruction model, the self-memorization

114 principle is introduced in Section 4. Model forecast experiments are described in
115 Section 5, and conclusions are given in Section 6.

116 **2. Research data and forecast factors**

117 **2.1 Data**

118 The monthly average SST data were obtained from the UK Met Office Hadley
119 Centre for the region (30 °S-30 °N; 120 °E -90 °W). The gridded 1° × 1° Met Office
120 Hadley Sea Ice and SST dataset (HadISST1; Rayner et al. 2003) includes both in situ
121 and available satellite data. The sea areas provide important information on
122 ocean-atmosphere coupling in the East and West Pacific Ocean and the El Niño /La
123 Niña events. The reanalysis data, zonal winds and sea level pressures were obtained
124 from the National Center for Environmental Forecast of America and the National
125 Center for Atmospheric Research (Kalnay et al., 1996). The sea surface height (SSH)
126 field was obtained from Simple Ocean Data Assimilation (SODA) data (James and
127 Benjamin, 2008). Outgoing longwave radiation (OLR) was obtained from the
128 National Oceanic and Atmospheric Administration (NOAA) satellites, at a resolution
129 of 0.5° × 0.5° (Liebmann and Smith, 1996). The Southern Oscillation Index (SOI) data
130 were obtained from the Climate Prediction Center (CPC). The time series of all data
131 were from Jan. 1951 to Dec. 2010, 720 months in total.

132 **2.2 EOF deconstruction**

133 The sea surface temperature anomaly (SSTA) field can be calculated from the
134 SST field and can be deconstructed into time (coefficients)-space (structure) using the
135 empirical orthogonal function (EOF) method. Detailed information on the EOF

136 method can be seen in the related references (Dommenget & Latif, 2002). We have
137 used covariance matrix, because the covariance matrix was selected to diagnose the
138 primary patterns of co-variability in the basin-wide SSTs, rather than the patterns of
139 normalized covariance (or correlation matrix).

140 We used the smooths function with MATLAB to smooth the SSTA field before
141 the EOF deconstruction, which is five points two times moving, mainly filtering out
142 some noise points and outliers. Then an EOF analysis of smoothed anomalies was
143 performed, and the first two SSTA EOFs are shown in Figs. 1a and 1c. The principal
144 component (PC) time series corresponding to the first and second EOFs are shown in
145 Figs. 1b and 1d. The first EOF pattern, which accounted for 61.33% of the total SSTA
146 variance, represented the mature ENSO phase (El Niño or La Niña), and the
147 corresponding PC time series was highly correlated (with a correlation coefficient of
148 0.85) with the cold tongue index (SST anomaly averaged over 4°S – 4°N , 180° – 90°
149 W) over the whole period. The second EOF, accounting for 14.52% of the total
150 SSTA variance, indicated the ENSO signal beginning to enhance. Compared with the
151 first mode, these were slightly attenuated in terms of the scope and intensity. The
152 above analysis is similar to the EOF analysis of the SSTA field in the previous studies
153 (Johnson et al., 2000; Timmermann et al., 2001). This indicates that the front two
154 variance contribution modes can describe the main characteristics of the SSTA field
155 and El Niño/La Niña. Therefore, we can choose the T_1, T_2 time series EOF
156 decomposition modes as the modelling objects.

157 **2.3 Selection of other prediction model factors**

158 Considering the complexity of computation, the amount of variables in the
159 equations of our model can't be too large, usually 3 or 4 for the best. This has been
160 explained in our previous studies (Zhang et al., 2006; Zhang et al., 2008). If there are
161 more than 4 variables in the modeling equation, it will cause the amount of
162 parameters such as $a_1, a_2, \dots, a_n, b_1, b_2, \dots, b_n, \dots$ too large. The huge computation makes it
163 difficult to be precisely modeled. Thus, the total number of parameters in the model of
164 five variables was 102, which may cause an overfitting problem. Hence, when we
165 selected the model of five or six variables which entailed large amounts of
166 computation that made precision difficult, and too many parameters might cause an
167 overfitting phenomenon. If we choose only two or even fewer variables, the forecast
168 performance is poor too. Too few variables cause too small reconstructed parameters,
169 resulting in amounts of important information missing out in the model. Thus, four
170 variables are best for dynamically and accurately modeling. Because we have chosen
171 two time series in section 2.2 as the modeling objects, now we should select the other
172 two ENSO intensity impact factors.

173 The ENSO intensity impact factor is an important issue in ENSO prediction.
174 Previous studies have been completed in this area, which found that teleconnection
175 patterns, temperature, precipitation, wind and SSH may affect ENSO strength. For
176 example, Trenberth et al. (1998) noted that PNA, SOI and OLR in the Pacific
177 Intertropical Convergence Zone (ITCZ) are all closely related to ENSO.
178 Webster (1999) pointed out after the 1970, Indian Ocean dipole (IOD) is not only
179 affected by ENSO, but also affected the strength of ENSO (Ashok et al., 2001). Yoon

180 and Yeh (2010) reported that the Pacific Decadal Oscillation (PDO) disrupts the
181 linkage between El Niño and the following Northeast Asian summer monsoon
182 (NEASM) through inducing the Eurasian pattern in the mid-high latitudes. The vast
183 majority of studies (Tomita and Yasunari, 1996; Zhou and Wu, 2010; Kim et al., 2017)
184 have concentrated on the impacts of ENSO on the East Asian winter
185 monsoon (EAWM). During the EAWM season, ENSO generally reaches its mature
186 phase and has the most prominent impact on the climate. Wang et al. (1999a) and
187 Wang et al. (1999b) suggested that the zonal wind factors in the eastern and western
188 equatorial Pacific play a critical role in the phase of transition of the ENSO cycle,
189 which could excite eastward propagating Kelvin waves and affect the SSTA in the
190 equatorial Pacific. Zhao et al. (2012) analyzed the characteristics of the tropical
191 Pacific SSH field and its impact on ENSO events.

192 Based on the above analysis, we have selected nine factors, which may be
193 closely related with the ENSO index (Niño3.4).

194 (1) The zonal wind in the eastern equatorial Pacific factor (u1) was calculated
195 as the grid-point average of zonal wind in the area [5°S ~ 5°N, 150°W ~ 90°W].

196 (2) The zonal wind in the western equatorial Pacific factor (u2) was calculated
197 as the grid-point average of zonal wind in the area [0° ~ 10°N; 135°E ~ 180°E].

198 (3) The PNA teleconnection factor was obtained from the CPC.

199 (4) the dipole mode index factor (DMI) was obtained from SSTA for
200 June-July-August (JJA) based on Saji(1999) method.

201 (5) The SOI factor was obtained from the CPC.

202 (6) The PDOI factor was obtained from department of Atmospheric Sciences
203 in the university of Washington. The web is
204 <http://tao.atmos.washinton.edu/pdo/RDO.latest>.

205 (7) The EAWM index (EAWMI) factor was proposed by Yang et al. (2002),
206 which is defined by the meridional 850-hPa winds averaged over the region (20°
207 $\sim 40^{\circ}$ N, $100^{\circ} \sim 140^{\circ}$ E).

208 (8) The OLR in the ITCZ factor was calculated as the grid-point average of
209 OLR in the area [10° N $\sim 20^{\circ}$ N, 120° E $\sim 150^{\circ}$ E].

210 (9) The SSH factor was calculated as the grid-point average of the SSH data in
211 the area [10° S $\sim 10^{\circ}$ N; 120° E $\sim 60^{\circ}$ W].

212 A correlation analysis of the above factors was carried out and the results are
213 shown in Table 1.

214 Table 1 shows that SOI and EAWMI have the stronger correlation with the
215 front two time series T_1, T_2 than the other 7 factors. The results are also consistent with
216 previous research (Clarke and Van Gorder, 2003; Drosdowsky, 2006; Zhang et al.,
217 1996; Wang et al., 2008; Yang and Lu, 2014). Therefore, the first time series T_1 , the
218 second time series T_2 , SOI and EAWMI will be selected as prediction model factors.

219 **3. Reconstruction of dynamical model based on GA**

220 Takens' delay embedding theorem (Takens, 1981) provides the conditions under
221 which a smooth attractor can be constructed from observations made with a generic
222 function. Later results replaced the smooth attractor with a set of arbitrary
223 box-counting dimensions and the class of generic functions with other classes of

224 functions. Takens had shown that if we measured any single variable with sufficient
 225 accuracy for a long period of time, it would be possible to construct the underlying
 226 dynamical structure of the entire system from the behavior of that single variable
 227 using delay coordinates and the embedding procedure. It was therefore possible to
 228 construct a dynamical model of system evolution from the observed time series.
 229 Introducing this idea here, four time series of the T_1 , T_2 , SOI and EAWMI factors
 230 were chosen to construct the dynamical model.

231 The basic idea of statistical-dynamical model construction is discussed in
 232 Appendix A and was introduced in our previous work (Zhang et al., 2006; Hong et al.,
 233 2014).

234 A simplified second-order nonlinear dynamical model can be used to depict the
 235 basic characteristics of atmosphere and ocean interactions (Fraedrich, 1987). Suppose
 236 that the following nonlinear second-order ordinary differential equations are taken as
 237 the dynamical model of reconstruction. In the equations, x_1, x_2, x_3, x_4 were used to
 238 represent the time coefficient series of T_1 , T_2 , SOI and EAWMI.

$$\begin{aligned}
 \frac{dx_1}{dt} &= a_1x_1 + a_2x_2 + a_3x_3 + a_4x_4 + a_5x_1^2 + a_6x_2^2 + a_7x_3^2 + a_8x_4^2 + a_9x_1x_2 + a_{10}x_1x_3 + a_{11}x_1x_4 + a_{12}x_2x_3 + a_{13}x_2x_4 + a_{14}x_3x_4 \\
 \frac{dx_2}{dt} &= b_1x_1 + b_2x_2 + b_3x_3 + b_4x_4 + b_5x_1^2 + b_6x_2^2 + b_7x_3^2 + b_8x_4^2 + b_9x_1x_2 + b_{10}x_1x_3 + b_{11}x_1x_4 + b_{12}x_2x_3 + b_{13}x_2x_4 + b_{14}x_3x_4 \\
 \frac{dx_3}{dt} &= c_1x_1 + c_2x_2 + c_3x_3 + c_4x_4 + c_5x_1^2 + c_6x_2^2 + c_7x_3^2 + c_8x_4^2 + c_9x_1x_2 + c_{10}x_1x_3 + c_{11}x_1x_4 + c_{12}x_2x_3 + c_{13}x_2x_4 + c_{14}x_3x_4 \\
 \frac{dx_4}{dt} &= d_1x_1 + d_2x_2 + d_3x_3 + d_4x_4 + d_5x_1^2 + d_6x_2^2 + d_7x_3^2 + d_8x_4^2 + d_9x_1x_2 + d_{10}x_1x_3 + d_{11}x_1x_4 + d_{12}x_2x_3 + d_{13}x_2x_4 + d_{14}x_3x_4
 \end{aligned}
 \tag{1}$$

242 Based on the parameter optimization search method of GA in Appendix A, the

243 time coefficient series of T_1 , T_2 , SOI and EAWMI from January 1951 to April 2008
 244 are chosen as the expected data to optimize and retrieve model parameters. In order to
 245 eliminate the dimensionless relationship between variables, data standardization

246 $x_{nor} = \frac{x - x_{min}}{x_{max} - x_{min}}$ is to transform data from different orders of magnitude to the same

247 order of magnitude, ~~thus making the data comparable. So we used $x_{nor} = \frac{x - x_{min}}{x_{max} - x_{min}}$~~

248 ~~to normalize the raw value of each of the four predictors, then we used the normalized~~

249 ~~value to model and forecast.~~ Finally, we made forecast results revert back to the raw

250 data magnitude by $x = x_{nor}(x_{max} - x_{min}) + x_{min}$.

251 In order to quantitatively compare the relative contribution of each item of our
 252 model to the evolution of the system, we calculated the relative variance contribution.

253 The formula is as follows: $R_i = \frac{1}{n} \sum_{j=1}^n [\frac{T_i^2}{\sum_{i=1}^{14} T_i^2}]$, $i = 1, 2, \dots, 14$, Where n is the length of

254 the data, $T_i = a_1x_1, a_2x_2, \dots, a_{14}x_3x_4$ is the item in the equation. According to our

255 previous research (Hong et al., 2007), the variance contribution of the real item

256 reflecting the performance of the model has a large proportion, while the variance

257 contribution of the false term is almost zero, so we delete the weak items of

258 $R_i < 0.01$.

259 After deleting the weak items, the nonlinear dynamical model of the first time
 260 series T_1 , the second time series T_2 , SOI and EAWMI can be reconstructed as follows:

$$\begin{aligned}
\frac{dx_1}{dt} &= F_1 = -0.3328x_1 + 1.2574x_2 - 0.3511x_3 - 0.0289x_1^2 + 3.1280x_3^2 + 0.0125x_1x_2 + 2.7805x_1x_3 - 1.5408x_2x_4 \\
\frac{dx_2}{dt} &= F_2 = 1.0307x_1 - 3.1428x_2 + 0.3095x_4 + 4.2301x_1^2 - 1.2066x_2^2 + 2.5024x_4^2 - 0.2891x_1x_3 + 0.7815x_1x_4 - 0.4266x_3x_4 \\
\frac{dx_3}{dt} &= F_3 = -2.3155x_1 + 3.2166x_3 + 1.5284x_4 - 1.4527x_2^2 - 0.0034x_3^2 - 4.1206x_4^2 - 0.0025x_1x_4 + 0.0277x_2x_3 + 1.2860x_2x_4 \\
\frac{dx_4}{dt} &= F_4 = 0.4478x_2 - 0.0268x_4 + 0.8995x_1^2 - 2.3890x_3^2 + 0.2037x_4^2 + 1.3035x_1x_2 + 2.0458x_1x_4 - 2.0015x_2x_4
\end{aligned}
\tag{2}$$

The model required testing. Because the training period was from January 1951 to April 2008, we chose T_1 , T_2 , SOI and EAWMI of May 2008, which were not used as initial forecast data in the modeling. Next, the Runge–Kutta method was used to do the numerical integration of the above equations, and every step of the integration was regarded as 1 month’s worth of forecasting results. As a result, forecast results of four time series over a period of 20 months were obtained. Here, the focus was on the forecast results of T_1 and T_2 , as shown in Fig.2.

The pearson correlation coefficient (CC) (Wang et al. 2009b) and the mean absolute percentage error (MAPE)(Hu et al. 2001) are employed as objective functions to calibrate the model. The CC evaluates the linear relationship between the observed and predicting values and MAPE measures the difference between the observed and predicting values.

From Fig. 2, forecast performance of T_1 and T_2 within 5 months was better. Using T_1 as an example, the CC between model predictions and corresponding observations over the first five months forecasts was 0.8966 and MAPE was 8.32%. However, after 5 months, MAPE increased rapidly, and was 31.29% at 10 months. The model forecast then significantly diverged from observations, and the forecast became inaccurate. After 10 months, the forecast results became increasingly worse,

281 which indicated that the forecast of the model after 5 months was unacceptable. The
282 forecast results of T_2 were similar to those of T_1 .

283 The model's skill should be further assessed by cross-validated retroactive
284 hindcasts of the time series. As in the above example, omitting a portion of the time
285 series (12 months, Jan. 1951 to Dec. 1951) from observations, we trained the model
286 based on the data from Jan. 1951 to Dec. 2010, and then predicted the omitted
287 segments (12 months, Jan. 1951 to Dec. 1951). Then in the next prediction
288 experiment, the omitted segment is Jan. 1952 to Dec. 1952 and the training samples
289 are Jan. 1951 to Dec. 1951 and Jan. 1953 to Dec. 2010. So the forecast time series is
290 Jan. 1952 to Dec. 1952. We then repeated this procedure by moving the omitted
291 segment along the entirety of the available time series. Each experiment has used the
292 different training sample and ~~have~~ established the different model equation (but the
293 method is the same). The similar process of the cross-validated retroactive hindcasts
294 has also been used in the previous literatures (Hu et al., 2017).

295 Finally, we obtained cross-validated retroactive hindcast results of T_1 and T_2 , as
296 shown in Fig. 3. So the forecast results of 60 cross experiment (each experiment is the
297 prediction of the 12 month as Fig.2) according to the time sequence can merger into a
298 new time series (from Jan.1951-Dec.2010), and then ~~the pearson correlation~~
299 ~~coefficient (CC)~~ and ~~the mean absolute percentage error (MAPE)~~ can be calculated
300 by the new prediction time series and the time series of the actual value. Figure 3 is
301 combined results of the 60 forecast experiments.

302 As Fig. 2, the forecast performance of T_1 and T_2 in Fig. 3 was not satisfactory.

303 The model forecast significantly diverged from observations, and the forecast became
304 inaccurate. The CC of T_1 and T_2 between model predictions and corresponding
305 observations were 0.3411 and 0.4176, respectively. Additionally, the MAPE of T_1 and
306 T_2 were 65.42% and 57.56%, respectively. This indicates that the forecast of the model
307 in the long-term was inaccurate and unacceptable.

308 The forecast result may be inaccurate when the integral forecasting time is long.
309 There will be a significant divergence which will cause an ineffective forecast. To
310 improve the forecast accuracy, the forecast not only depends on the integral equation
311 but also on a single initial value. Choosing the different initial value will cause
312 different forecast accuracy. For example, in a total of 60 cross-validated retroactive
313 hindcasts examples, the minimum MAPE was 37.65%, while the maximum MAPE
314 was 89.88%. A forecast, depending on a single initial value, will cause instability of
315 the forecast results. These two problems are addressed by introducing the
316 self-memorization principle in the next section.

317

318 **4. Introduction of self-memorization dynamics to improve the** 319 **reconstructed model**

320 In the above discussion, it was shown that the accuracy of the forecast results of
321 equation (2) were unsatisfactory. To improve long-term forecasting results, the
322 principle of self-memorization can be introduced into the mature model (Gu, 1998;
323 Chen et al., 2009). The principle of self-memorization dynamics (Cao, 1993; Feng et
324 al., 2001) can be seen in Appendix B.

325 Based on Eq. (B10) in Appendix B, the improved model can be expressed as

326

$$\text{follows: } \begin{cases} x_{1t} = \sum_{i=-p-1}^{-1} \alpha_{1i} y_{1i} + \sum_{i=-p}^0 \theta_{1i} F_1(x_{1i}, x_{2i}, x_{3i}, x_{4i}) \\ x_{2t} = \sum_{i=-p-1}^{-1} \alpha_{2i} y_{2i} + \sum_{i=-p}^0 \theta_{2i} F_2(x_{1i}, x_{2i}, x_{3i}, x_{4i}) \\ x_{3t} = \sum_{i=-p-1}^{-1} \alpha_{3i} y_{3i} + \sum_{i=-p}^0 \theta_{3i} F_3(x_{1i}, x_{2i}, x_{3i}, x_{4i}) \\ x_{4t} = \sum_{i=-p-1}^{-1} \alpha_{4i} y_{4i} + \sum_{i=-p}^0 \theta_{4i} F_4(x_{1i}, x_{2i}, x_{3i}, x_{4i}) \end{cases} \quad (3)$$

327

where y_i is replaced by the mean of two values at adjoining times; i.e.,

328

$$y_i \equiv \frac{1}{2}(x_{i+1} + x_i); F \text{ is the ~~dynamic~~dynamical core of the self-memorization equation,$$

329

which can be obtained from Eq. (2); and α and θ are the memory coefficients, the

330

formula for which can be found in Appendix B.

331

If the values of α and θ can be obtained, Eq. (3) can be used to obtain the

332

results of final prediction. The memory coefficients α and θ in Eq. (3) were

333

calibrated using the least-squares method with the same data (January 1951 to April

334

2008) as those used in Section 3. Eq. (3) can be deconstructed as follows (M is the

335

length of the time series):

336

$$X = \begin{bmatrix} x_{11} \\ x_{12} \\ \cdot \\ \cdot \\ \cdot \\ x_{1M} \end{bmatrix}, \alpha = \begin{bmatrix} \alpha_{-p-1} \\ \alpha_{-p} \\ \cdot \\ \cdot \\ \cdot \\ \alpha_{-1} \end{bmatrix}, Y = \begin{bmatrix} y_{-p-1,1} & y_{-p,1} & \cdots & y_{-1,1} \\ y_{-p-1,2} & y_{-p,2} & \cdots & y_{-1,2} \\ \cdot & \cdot & & \cdot \\ \cdot & \cdot & & \cdot \\ \cdot & \cdot & & \cdot \\ y_{-p-1,M} & y_{-p,M} & \cdots & y_{-1,M} \end{bmatrix}, \Theta = \begin{bmatrix} \theta_{-p} \\ \theta_{-p+1} \\ \cdot \\ \cdot \\ \cdot \\ \theta_0 \end{bmatrix},$$

337

$$F = \begin{bmatrix} F_{-p,1} & F_{-p+1,1} & \cdots & F_{0,1} \\ F_{-p,2} & F_{-p+1,2} & \cdots & F_{0,2} \\ \cdot & \cdot & & \cdot \\ \cdot & \cdot & & \cdot \\ \cdot & \cdot & & \cdot \\ F_{-p,M} & F_{-p+1,M} & \cdots & F_{0,M} \end{bmatrix}$$

338 The matrix equation is:

$$339 \quad X = Y\alpha + F\theta \quad (4)$$

$$340 \quad \text{where } Z = [Y:F], \quad W = \begin{bmatrix} \alpha \\ \vdots \\ \theta \end{bmatrix} .$$

341 Eq. (4) can be written as:

$$342 \quad X = ZW \quad (5)$$

343 The memory coefficients vector W can be calibrated using the least squares
344 method:

$$345 \quad W = (Z^T Z)^{-1} Z^T X \quad (6)$$

346 The memory coefficients a, θ can be obtained from Eq. (6). We then made a
347 prediction using the self- memorization equation (3), which used the p values before
348 t_0 .

349 The coefficients in F and W were used with the same training data from January
350 1951 to April 2008. In the forecast examples, we trained both the coefficients in F and
351 W at the same time, but in the paper we describe them separately to facilitate the
352 reader for better understanding.

353 **5. Model prediction experiments**

354 **5.1 Forecast of time series T_1 and T_2**

355 The training sample for the model was from January 1951 to April 2008. Here, from
356 Eq. (3), the forecast results using T_1, T_2 , SOI and EAWMI factors can be calculated, called
357 as step-by-step forecast.

358 When the retrospective order p is confirmed, step-by-step forecasts can be

359 carried out. For example, when the T_1, T_2 , SOI and EAWMI values of May 2008 were
360 forecast, y_i was obtained from the previous $p + 1$ time of T_1, T_2 , the SOI and the
361 EAWMI data, and $F_i(x_{1i}, x_{2i}, x_{3i}, x_{4i})$ was obtained from the previous p times of
362 T_1, T_2 , the SOI and the EAWMI data. All four equations were integrated simultaneously.
363 Taking these in Eq. (3), we can get the T_1, T_2 , SOI and EAWMI values of May 2008,
364 which these can be taken as the initial values for the next prediction step. Then, the
365 T_1, T_2 , SOI and EAWMI values from June 2008 and so on, can be generated.

366 5.1.1 Determination of p

367 Based on the self-memorization principle, the self-memorization of the system
368 determines the retrospective order p (Cao, 1993). If the system forgets slowly,
369 parameters a and θ will be small and the p value should be high. The SSTA field
370 forecasts were on a monthly scale, the change of which was slow in contrast to
371 large-scale atmospheric motion. So parameters a and θ were small, and generally,
372 the p value was in the range 5 to 15 (Cao, 1993).

373 The retrospective order p was obtained by a trial calculation method. We selected
374 the p values in the range 4 to 16 to construct the model. The CC and MAPE of
375 long-term fitting test (from February 1951 to December 2010) are shown in Table 2,
376 which can be used as the standard to determine the retrospective order p .

377 Table 2 indicates that when $p = 6$, the MAPE values of long-term fitting test
378 were the smallest and the CCs were the largest. Also, when p from 5 to 9, The CCs
379 were all more than 0.58 and the forecast results were all good, which is consistent
380 with our interpretation of the physical mechanisms in section 6.2 below. SOI and

381 EMWMI were 5-12 months lead relationships with SST (Xu et al., 1993; Chen et al,
382 2010; Wang et al., 2003). Using a cumulative period of SOI, EMWMI 5-8 months
383 ahead as initial values can help improve the final forecast results. Our results in table
384 2 are consistent with the actual physical ENSO process. Therefore, we selected the
385 retrospective order as $p=6$.

386 Then, the prediction experiments can be carried out, based on improved
387 self-memorization Eq. (3).

388 The improved self-memorization equation of T_1, T_2 , SOI and EAWMI can then be
389 established. After the differential equation was discretely dealt with, the memory
390 coefficients were solved by the least-squares method given in section 4 (Training
391 period is January 1951 to April 2008). Finally, the improved prediction equation of
392 T_1, T_2 , SOI and EAWMI, based on the self-memorization principle, can be expressed
393 as:

$$394 \begin{cases} x_{1t} = \sum_{i=-7}^{-1} \alpha_{1i} y_{1i} + \sum_{i=-6}^0 \theta_{1i} F_1(x_{1i}, x_{2i}, x_{3i}, x_{4i}) \\ x_{2t} = \sum_{i=-7}^{-1} \alpha_{2i} y_{2i} + \sum_{i=-6}^0 \theta_{2i} F_2(x_{1i}, x_{2i}, x_{3i}, x_{4i}) \\ x_{3t} = \sum_{i=-7}^{-1} \alpha_{3i} y_{3i} + \sum_{i=-6}^0 \theta_{3i} F_3(x_{1i}, x_{2i}, x_{3i}, x_{4i}) \\ x_{4t} = \sum_{i=-7}^{-1} \alpha_{4i} y_{4i} + \sum_{i=-6}^0 \theta_{4i} F_4(x_{1i}, x_{2i}, x_{3i}, x_{4i}) \end{cases} \quad (7)$$

395 where

$$396 \alpha = [\alpha_{ij}] = \begin{bmatrix} 0.0315 & -2.113 & 0.0284 & 2.1468 & 0.0688 & -0.7014 & 1.3248 \\ 0.4088 & -1.887 & -1.0233 & 1.5485 & 0.9028 & 1.0255 & -0.6443 \\ -0.9088 & -0.2557 & 0.9671 & -0.0054 & 1.0568 & 2.9764 & -0.5234 \\ 0.2088 & -1.0567 & 0.4891 & -0.5066 & -0.4890 & 1.4555 & 1.0966 \end{bmatrix}$$

($i = 0, 1, \dots, 4; j = -7, -6, \dots, -1$)

$$\theta = [\theta_{ij}] = \begin{bmatrix} 0.0485 & 0.0425 & -1.7688 & 0.8543 & 2.8901 & -0.1788 & -0.9066 \\ 0.07642 & 0.0941 & -1.2466 & -0.2288 & 0.1097 & 2.3221 & -1.4228 \\ -0.5288 & 1.2368 & -0.5568 & -0.0155 & 0.2886 & -0.1560 & 1.2775 \\ 1.5335 & -0.2887 & -0.5336 & -0.6072 & -0.5611 & 1.0225 & -1.0625 \end{bmatrix}$$

$(i = 0, 1, \dots, 4; j = -6, -5, \dots, 0)$

398 The step-by-step forecast was performed. The retrospective order $p = 6$ means
 399 that earlier seven observation data ($p + 1 = 7$) should be used during the forecasting
 400 process. The forecast results per month were saved for the next period predictions.

401 5.1.2 Long-term step-by-step forecasts of T_1 and T_2

402 To test the actual forecast performance of the above improved model, long-term
 403 step-by-step forecasts of T_1 and T_2 from May 2008 to December 2010 for 20 months
 404 were carried out, as shown in Fig. 4. The forecast results of T_1 and T_2 were good.
 405 Within 8 months, the CCs of T_1 and T_2 were 0.9163 and 0.9187. MAPEs of T_1 and
 406 T_2 were small, only 5.86% and 6.78%. The forecast time series from 8 months to 14
 407 months gradually diverged, but the trend was acceptable. The CCs of T_1 and T_2
 408 reached 0.8375 and 0.8251, and MAPEs of T_1 and T_2 were 8.32% and 9.11%. After
 409 14 months, forecast began to diverge and the error started to increase, but the CCs of
 410 T_1 and T_2 remained about 0.6899 and 0.6782, and MAPEs reached 18.31% and
 411 19.44%, which can be acceptable.

412 5.2 Cross-validated retroactive hindcasts of time series T_1 and T_2

413 As in section 3, the model's skill should be further assessed by cross-validated
 414 retroactive hindcasts of the time series. Because our step-by-step forecasts need the
 415 earlier seven observation data ($p + 1 = 7$), we can obtain cross-validated retroactive
 416 hindcast results of T_1 and T_2 from August 1951 to December 2010, as shown in Fig.

417 5.

418 From Fig. 5, the forecast performance of T_1 and T_2 was good. The CCs of
419 T_1 and T_2 were 0.7124 and 0.7036, respectively. The MAPEs of T_1 and T_2 were
420 small, only 19.57% and 19.79%, respectively. The peaks and valleys of T_1 and T_2
421 were also forecasted accurately. The forecast results indicated that the cross-validated
422 retroactive hindcast results of T_1 and T_2 were close to the observed values.
423 Compared to Fig. 3, the improved model had better forecast abilities than the original
424 model.

425 Many researchers (Zhang et al., 2003b; Smith, 2004) have used Oceanic Niño
426 Index (ONI) which is used by the U.S. NOAA Climate Prediction Center to determine
427 the El Niño and La Niña years. It defined that the ONIs of five consecutive months in
428 winter were all more than 0.5 (less than -0.5) is the El Niño (La Niña) year. Based on
429 the above criterion, we can divide the total 60 years (1951-2010) into three categories.
430 It includes the 18 examples of El Niño year (such as 1958, 1964, 1966, etc.), 22
431 examples of La Niña year (such as 1951, 1955, 1956, etc.) and the remaining 20
432 experiments of the neutral year. Since the details in Fig.5 is not clear, we list the
433 forecast results of 60 experiments (including 18 El Niño examples, 22 La Niña
434 examples and 20 Neutral examples) in table 3.

435 From table 3, the average of CC of both T_1 and T_2 of 60 experiments within
436 6 months was more than 0.84 and MAPE was less than 8%. The average of CC within
437 12 months was more than 0.74 and MAPE was less than 12%. According to the
438 literature (Barranel et al., 1999), when MAPE was less than 15%, which means the
439 error was not great and the forecast results were good. Obviously, the forecast results

440 of El Niño / La Niña experiments were a little worse than those of neutral examples,
441 which means the forecast ability of our model for the abnormal situation was a little
442 worse than those for the normal situation. But even for El Niño / La Niña experiments,
443 the average of CC was still more than 0.7 and MAPE was less than 15%, which
444 means the error was not too large and was still within an acceptable range.

445 **5.3 Forecast of the SSTA field**

446 When we obtained the forecast results of the time coefficient series T_1 and T_2 ,
447 we submitted them into the following equation to reconstruct the forecast SSTA field:

$$448 \quad \hat{x}_t = \sum_{n=1}^2 E_n \bullet T_n, t = 1, 2, \dots, 12 \quad (8)$$

449 where E_n , T_n are the EOF space fields and forecast time coefficients,
450 respectively, and \hat{x}_{ij} is the forecast SSTA field reconstructed by EOF.

451 After reconstruction of the space mode (treated as constant) and time coefficient
452 series (model prediction), the forecast of the SSTA fields was obtained, based on the
453 forecast results of T_1 and T_2 in Section 5.2. For economy of space, we cannot draw
454 all of the forecasted SSTA fields, so we selected a strong El Niño event (December
455 1997), a strong La Niña event (December 1999) and a neutral event (November 2002)
456 as examples.

457 Fig. 6 shows the forecast SSTA field during a strong El Niño event. From the
458 actual SSTA field in December 1997 (Fig. 6a), an obvious warm tongue structure
459 occurred in the area of [10°S~5°N, 90°W~150°W] in the Eastern Equatorial Pacific,
460 and a warm anomalous distribution arose in the west Pacific, which indicated a weak
461 El Niño event. The forecasted SSTA field of December 1997 is shown in Fig. 6b.
462 Although the range of warm tongue was a little bigger than the actual situation, the

463 forecast shape was similar to the actual field and also the contour lines were similar.
464 The average MAPE between the forecast field and the actual field is 8.56%, which
465 was controlled within 10%. The forecast results of the improved model event were
466 quite good for the El Niño event.

467 Fig.7 shows the forecasted SSTA field of a strong La Niña event. From the actual
468 SSTA field in December 1999 (Fig. 7a), an obvious cold pool occurred in the area of
469 [10 °S~10 °N, 120 °W~180 °W] in the Equatorial Pacific, which covered the Niño3.4
470 area. This SSTA field presented a strong strength La Niña event. The forecast SSTA
471 field from December 1999 is shown as Fig. 7b. Although the strength of the cold pool
472 was weaker than the actual situation, the forecast shape was similar to that of the
473 actual field. The average MAPE between the forecast field and the actual field was
474 9.69%. The errors were larger than that of the El Niño event, but they can be
475 controlled within 10%, which is acceptable.

476 Fig. 8 shows the forecasted SSTA field of a neutral event. From the actual SSTA
477 field in November 2002 (Fig. 8a), a warm pool occurred in the area of [10 °S~10 °N,
478 120 °W~180 °W] in the Equatorial Pacific, which covered the Niño3.4 area. However,
479 the warm pool was small and weak, which represented a neutral event. The forecasted
480 SSTA field from November 2002 is shown in Fig. 8b. Comparing Figures 6, 7 and 8,
481 we can see that the forecasted SSTA field of a neutral event was a little worse than
482 that of the El Niño and La Niña events. The forecasted shape of the SSTA field
483 basically described the actual situation, but the warm pool in the Niño3.4 area was
484 stronger and bigger than that of the actual situation, which indicated a borderline El

485 Niño event. The average MAPE between the forecasted field and the actual field was
486 14.50%, which was big but can be accepted.

487 We obtained the average values of MAPE of 18 El Niño events, 22 La Niña
488 events and 20 neutral events, which were 9.52%, 9.88% and 14.67%, respectively,
489 representing a good SSTA field forecasting ability of our model.

490 **5.4 Forecast of ENSO index**

491 The ENSO index can be represented as the sea surface temperature anomaly
492 (SSTA) in the Niño-3.4 region (5°N - 5°S , 120° - 170°W) and the ENSO index
493 forecast was the 3-month forecast (Barnston et al. 2012). So we also can pick up the
494 ENSO index from the above forecasted SSTA field. The forecast results of the ENSO
495 index within 20 months can also be obtained. The definition of lead time can be seen
496 in the reference (Barnston et al. 2012). Therefore, similar to the forecast experiment in
497 section 5.1, a succession of running 3-month mean SST anomalies with respect to the
498 climatological means for the respective prediction periods, averaged over the Niño 3.4
499 region, can be obtained, as demonstrated in Fig. 9.

500 The evaluation criteria of the ENSO index is the temporal correlation (TC), its
501 definition and specific calculation steps can be seen in these literatures (Kathrin et
502 al.,2016; Nicosia et al. 2013); The TC is often used to measure the prediction effect of
503 the ENSO index. For example, Barnston et al.in 2012 also used the TC to compare the
504 forecast skill of 21 real-time seasonal ENSO models.

505 The forecast results within lead times of 18 months are shown in Fig. 9, which
506 demonstrate that the forecast results of the ENSO index are good. Within lead time of

507 12 months, the TC was 0.8985 and the MAPE value was small, only 8.91%. In
508 addition, the borderline La Niña event in 2008–2009 was predicted well. After lead
509 times of 12 months, forecasts began to diverge and the errors started to increase.
510 Although the TC remained approximately 0.61, MAPE reached 18.58%. Therefore, a
511 moderate strength El Niño event that occurred in 2009/10 was not predicted.

512 We should give more examples to test the ENSO prediction ability of our model.
513 As in section 5.3, we can divide 60 examples as three types, which are examples of
514 El Niño year, La Niña year and neutral year. Finally, we can obtain the forecast results
515 of different types of examples in different lead times, as shown in table 4.

516 From table 4, the average TC of 60 experiments was 0.712 and the average
517 MAPE was 7.62% within 12 months for all seasons of lead time, which indicates that
518 the overall ENSO forecast ability of our model was good. The forecast results of the
519 El Niño examples were significantly worse than those of La Niña examples, while the
520 forecast results of La Niña examples were significantly worse than those of neutral
521 examples, which show the model forecast ability of the abnormal state was worse than
522 the normal state of the ENSO index. Even for the forecast results of El Niño examples,
523 the average TC was still above 0.6 and the average MAPE can be controlled below
524 10%, which means the forecast results were still in the acceptable range. Our model
525 not only accurately predicted the stronger El Niño and La Niña phases but also the
526 neutral states.

527 The ENSO forecast often had a spring predictability barrier (Webster, 1999),
528 which was most prominent during decades of relatively poor predictability

529 (Balmaseda et al., 1995). To test our model, the skill should be computed over the
530 entire time series and separately for seasonal subsets of the time series. From the
531 table4, we can see that although the forecast results of the present model in the spring
532 were worse than in the autumn, the margin was not high, which means the model can
533 overcome the “spring predictability barrier,” to some extent.

534 **5.5 Compared with six mature models**

535 Barnston et al. (2012) compared many ENSO forecast models. Based on his
536 research, we selected four high quality dynamical models, including ECMWF, JMA,
537 the National Aeronautics and Space Administration Global Modelling and
538 Assimilation Office (NASAGMAO) and the National Centre for Environmental
539 Prediction Climate Forecast System (NCEP CFS; Version1). Two high quality
540 statistical models also be selected, including the University of California, Los Angeles
541 Theoretical Climate Dynamics (UCLA-TCD) multilevel regression model and the
542 NOAA/NCEP/CPC constructed Analogue (CA) model. The detail of the above
543 models can be seen in these references (Reynolds al., 2002; Luo et al., 2005; Barnston
544 et al., 2012).

545 We then compared the forecast ability of the above six models with that of our
546 model. All of the experiments of our model and six other models were conducted
547 under the same conditions using the same historical data for modelling and the same
548 initial values to forecast. In the CPC website, there are detailed explanations of six
549 models’ training samples and the initial values. So we do not need to install all these
550 models on their own machines and run them for forecasting. We just made training

551 samples and initial values of our model were the same with those of selected six
552 models. At an 8-month lead time, the TC of our model for all seasons combined was
553 0.613 (Fig. 10). In brief, the forecast ability of the ECMWF model was slightly better
554 than that of our model but the ability of the other 5 models was worse than that of our
555 model. While, in regard to the forecast length, the TC within 12 months of our model
556 is greater than 0.6, which was superior to the ECMWF model. In addition, the forecast
557 results of the UCLA-TCD model and the CPC CA model reduced quickly after
558 5-month lead times, so the forecast ability of our model was more stable than them.

559 The root mean square error (RMSE) was also examined to assess the
560 performance of discrimination and calibration. Barnston et al. (2012) believed that all
561 seasonal RMSE values contributed equally to a seasonally combined RMSE. So we
562 drew figure 11 to show seasonally combined RMSE.

563 From Fig. 10 and Fig. 11, we can see the highest correlation tend to have
564 lower RMSE. So the RMSE of our model was slightly higher than that of ECMWF
565 model, but it was much lower than those of the other 5 models. Figure 11 and Figure
566 12 is the average TC and RMSE of the 240 experiments of compared with six mature
567 models, covers a variety of different types of ENSO and different lead time. So those
568 samples should be really representative.

569 **6. Conclusions and discussion**

570 **6.1 Conclusions**

571 A new forecasting model of the SSTA field was proposed based on a
572 ~~dynamic~~dynamical system reconstruction idea and the principle of

573 self-memorization. The approach of the present paper consisted of the following
574 steps:

575 (1) The SST field can be time (coefficients)-space (structure) deconstructed
576 using the EOF method. Take T_1 , T_2 , SOI and EAWMI and consider them as
577 trajectories of a set of four coupled quadratic differential equations based on the
578 dynamicdynamical system reconstruction idea. The parameters of this
579 dynamicdynamical model were estimated using a GA.

580 (2) The forecast results of the dynamicdynamical model can be improved by
581 the self-memorization principle. The memory coefficients in the improved
582 self-memorization model were obtained using the GA method.

583 (3) The long-term step-by-step forecast results and cross-validated
584 retroactive hindcast results of time series T_1 and T_2 are all found to be good, with the
585 CC of approximately 0.80 and the MAPE of less than 15%.

586 (4) The improved model was used to forecast the SSTA field. The
587 forecasted SSTA fields of three types of events are accurate. Not only is the forecast
588 shape similar to the actual field but also the contour lines are similar.

589 (5) The improved model was also used to forecast the ENSO index. The
590 average TC of 60 examples within 12 months is 0.712, and the MAPE value is small,
591 only 7.62%, which proves that the improved model has better forecasting results of
592 the ENSO index. Although the forecast results of the model in the summer were
593 worse than in the winter, the margin was not high, which means that the model can
594 overcome the spring predictability barrier to some extent. Finally, compared with the

595 six mature models, the new dynamical-statistical forecasting model has a scientific
596 significance and practical value for the SST in the eastern equatorial Pacific and El
597 Niño/La Niña event predictions.

598 **6.2 Discussion**

599 L'Heureux et al.(2013) reported that using different data sets and time periods,
600 the 2nd EOF is not stable, being entirely due to the strong trend. So we need to do
601 more experiments to prove that we choose the second mode of EOF to be appropriate,
602 and whether different time periods will make us forecast unstable or not. Our original
603 data is the monthly average SST data from January 1951 to Dec. 2010, which are 60
604 years. We will increase the length of the data for 20 years (Jan.1931 –Dec.2010), for
605 10 years (Jan.1941- Dec.2010) and decrease the length of the data for 10 years
606 (Jan.1961- Dec.2010), for 20 years (Jan.1971- Dec.2010). And then we use the same
607 method to reconstruct a model and forecast the ENSO index as section5.4.[The results](#)

608 ~~show .The prediction results are shown in the table5.~~

609 ~~From the table, we can see that~~ in the 60 experiments, ~~the prediction results of~~
610 ~~the data period increased by 20 years are the best, and the prediction results of the~~
611 ~~data period decreased by 20 years is the worst. This is because the more data we use,~~
612 ~~the more information it contain. But from the table we can also see~~ the difference
613 among forecast results of both TC and MAPE of five different sample data are less,
614 and no abnormal change suddenly worse or better appear. All these indicate that using
615 different data sets and time periods, even though may have a certain impact on the
616 pattern of the 2nd EOF, but the impact on our forecast is not great and it will not

617 make our forecast unstable.

618 Actually, how many variables and which variables are used in our model
619 become a key issue to be resolved. We are a complex four factor differential
620 equations coupling model. We are a complex coupled model of four factor differential
621 equations, so we are more concerned with the correlation between each other. The
622 correlation must be considered as an important criterion to select the factors, but in
623 order to further verify the correctness of the selection criterion, we have carried out
624 the prediction experiments (the 60 cross-validated retroactive hindcasts experiments
625 of the ENSO index for all seasons combined at lead times of 8 months) of different
626 variables.

627 We can see that for all the forecast results of the models of different variables,
628 the prediction results of T_1, T_2, SOI is the best among those of the three factors and the
629 prediction result of $T_1, T_2, SOI, EAWMI$ is the best among those of the four factors. But
630 the prediction result of $T_1, T_2, SOI, EAWMI$ is best among all, which proves that our
631 selection factors are correct. In our previous study (Hong et al., 2015), the model of
632 the Western Pacific subtropical high was established by using the correlations as a
633 criterion to select factors and their forecast results are also good. Now we use the
634 correlations as a criterion to select factors is also in line with our previous research.

635 ~~The definition of overfitting: The learned hypothesis may fit the training set~~
636 ~~very well, but fail to predict to new examples (fail to fit additional data or predict~~
637 ~~future observations reliably).~~

638 ~~The potential for overfitting depends not only on the number of parameters and~~

639 ~~data but also the conformability of the model structure with the data shape, and the~~
640 ~~magnitude of model error compared to the expected level of noise or error in the~~
641 ~~data(Burnham and Anderson, 2002). So there are many reasons causing the overfitting~~
642 ~~phenomenon. But this does not mean having many parameters relative to the number~~
643 ~~of observations inevitably causes the overfitting problem (Golbraikh et al., 2003).~~
644 ~~There is no evidence that more parameters will be certain to result in overfitting.~~

645 Based on the definition of overfitting and the previous studies(Golbraikh et al., 2003;
646 Everitt and Skron dal,2010), there is no evidence that more parameters will be certain
647 to result in overfitting. ~~we~~ We can judge whether a model is overfitting or not by the
648 accuracy of prediction results of independent samples (Golbraikh and Tropsha, 2002;
649 Qin and Li, 2006).

650 In the sample training, our model does not purposely pursue the high degree of
651 the training samples fitting and improve the effectiveness of the independent
652 generalization. In fact in our paper the forecast results of the ~~Crosscross~~-validated
653 retroactive hindcasts (section 5.2) and the independent samples validation (table3 and
654 table4) are both good. Especially, the independent samples validation of the ENSO
655 index as the table4, we have carried out the 240 independent sample validation
656 prediction of four seasons of different ENSO events and the coverage of independent
657 samples test is very wide. Moreover, compared with 6 mature prediction models, the
658 forecast results of our model are also good, which prove the overfitting problem does
659 not exist in our model. ~~According to the previous literature (Islam and Sivakumar,~~
660 ~~2002; Sivakumar et al.,2001), we can see that prediction principle and structure of the~~

661 ~~phase space reconstruction (PSR) of dynamical system is not the same with the~~
662 ~~traditional neural network and in the small sample situation the forecasting results of~~
663 ~~PSR model are better than those of the traditional neural network (Sivakumar et~~
664 ~~al., 2002), which can be verified in the independent sample test (table3 and table4).~~ So
665 according to the definition of overfitting, we can say the over fitting phenomenon
666 does not exist in our model.

667 Compared with the original model, why the improved model has good forecast
668 results and can overcome the spring predictability barrier to some extent are as follow:
669 Recently, many studies have pointed out that spring is the most unstable season of the
670 air - sea interaction and the error is likely to develop or grow in the spring, resulting in
671 the spring predictability barrier (Zhang et al, 2012; Philander et al., 1992). When the
672 original model uses the indexes in summer as the initial values to predict, the SOI
673 factor representing the air-sea interaction is most unstable in the spring and the
674 EMWMI factor does not have much influence on ENSO in summer, so the forecast
675 results using the indexes in summer as the initial values are certainly much worse than
676 those using the indexes in the winter as the initial values. That is why our original
677 model does not overcome the spring predictability barrier.

678 However, the introduction of the self-memorization dynamics principle can help
679 our model overcome the spring predictability barrier to some extent. Although the
680 lead time is still summer (such as JJA), the information of the initial value actually
681 contains the previous $p + 1$ month (in this case $p = 6$, which contains the information
682 of the previous seven months, including the information of T_1, T_2 , SOI, EMWMI

683 factor in winter (January, February), spring (March, April, May) and summer (June
684 and July)). From the dynamical analysis, in this situation, the information and
685 interaction relationship of four factors have been a long period (from winter to
686 summer) accumulated, containing much air-sea interaction processes and winter
687 monsoon continued abnormal information, so the forecast results of our improved
688 model will be much better than the original model which simply uses only one initial
689 value. That is why the improved model overcomes the spring predictability barrier to
690 some extent.

691 The forecast results of our model are good, but it still has some problems:

692 (1) The inclusion of these terms and the physical processes do these terms in
693 equation (2) represent are important, especially for the discussion of dynamical
694 characteristics of the dynamical model. But now we are difficult to give a clear
695 meaning. Now the main work of our paper is the prediction experiments of the model.
696 For the reason of time and length, this paper mainly discusses the prediction results of
697 the model. The physical processes do these terms represent and the discussion of the
698 dynamical characteristics of the model will be the focus of our next work. Before this,
699 we have also used the Takens' delay embedding theorem to reconstruct the dynamical
700 model of the Western Pacific subtropical high(WPSH). And Based on the
701 reconstructed dynamical model, dynamical characteristics of WPSH are analyzed and
702 an aberrance mechanism is developed, in which the external forcings resulting in the
703 WPSH anomalies are explored, which have been published (Hong et al., 2016). We
704 also study the bifurcation and catastrophe of the West Pacific subtropical high ridge

705 index of a nonlinear model (Hong et al., 2017). Based on our previous method and
706 work, our next work is to analyse the physical processes and the dynamical
707 characteristics of the SST field.

708 (2)The experiments in the present study have proven that the forecasting results
709 of the improved model are good for large-scale systems, such as ENSO events, and
710 the forecasting period has been extended. However, for small-scale systems, such as
711 Hurricanes, whether the forecast results could be improved using the present
712 improved model needs to be further verified.

713 (3) Our paper focuses primarily on these defined indices with T_1, T_2 to
714 reconstruct a prediction model. Maybe, we can select variables (predictor) based on
715 EOF analysis and our model may be a more physically oriented model. Maybe we can
716 learn from Yim et al. (2013; 2015) to draw correlation maps between these fields and
717 the SSTA field and select the predictors from physical considerations. All these above
718 questions require that a lot of experiments to be carried out.

719 These items will be our future work.

720

721 **Acknowledgments** This study was supported by the Chinese National Natural
722 Science Fund (no. BK20161464) of Jiangsu Province and the Chinese National
723 Natural Science Fund (nos. 41375002, 41075045, 41306010, 41571017, 51190091
724 and 41071018) , the Program for New Century Excellent Talents in University
725 (NCET-12-0262), the China Doctoral Program of Higher Education

726 (20120091110026), the Qing Lan Project, the Skeleton Young Teachers Program, and
 727 the Excellent Disciplines Leaders in Midlife-Youth Program of Nanjing University.

728

729 **APPENDIX A: THE PRINCIPLE OF DYNAMICAL MODEL**
 730 **RECONSTRUCTION**

731 Suppose that the physical law of a nonlinear system going by over time can be
 732 expressed as the following difference form:

$$733 \frac{q_i^{(j+1)\Delta t} - q_i^{(j-1)\Delta t}}{2\Delta t} = f_i(q_1^{j\Delta t}, q_2^{j\Delta t}, \dots, q_i^{j\Delta t}, \dots, q_N^{j\Delta t}) \quad j = 2, 3, \dots, M-1 \quad (A1)$$

734 where f_i is the generalized nonlinear function of $q_1, q_2, \dots, q_i, \dots, q_N$, N is the number
 735 of variables, and M is the length of observed data. $f_i(q_1^{j\Delta t}, q_2^{j\Delta t}, \dots, q_i^{j\Delta t}, \dots, q_N^{j\Delta t})$ can be assumed
 736 to contain two parts: G_{jk} representing the expanding items which contain variable
 737 q_i , P_{ik} just representing the corresponding parameters which are real numbers
 738 ($i = 1, 2, \dots, N$, $j = 1, 2, \dots, M$, $k = 1, 2, \dots, K$).

739 It can be supposed as follows:

$$740 f_i(q_1, q_2, \dots, q_n) = \sum_{k=1}^K G_{jk} P_{ik} \quad (A2)$$

741 $D = GP$ is the matrix form of Eq.(A2), in which

$$742 D = \begin{Bmatrix} d_1 \\ d_2 \\ \dots \\ d_M \end{Bmatrix} = \begin{Bmatrix} \frac{q_i^{3\Delta t} - q_i^{\Delta t}}{2\Delta t} \\ \frac{q_i^{4\Delta t} - q_i^{2\Delta t}}{2\Delta t} \\ \dots \\ \frac{q_i^{M\Delta t} - q_i^{(M-2)\Delta t}}{2\Delta t} \end{Bmatrix}, \quad G = \begin{Bmatrix} G_{11}, G_{12}, \dots, G_{1K} \\ G_{21}, G_{22}, \dots, G_{2,K} \\ \dots \\ G_{M1}, G_{M2}, \dots, G_{M,K} \end{Bmatrix}, \quad P = \begin{Bmatrix} P_{i1} \\ P_{i2} \\ \dots \\ P_{iK} \end{Bmatrix} \quad (A3)$$

743 Parameters of the above equation can be determined through inverting the
 744 observed data. Vector P which satisfies the above equation can be solved, based on a
 745 given vector D. Assuming q is unknown, it is a nonlinear system. However, assuming

746 P is unknown, it is a linear system.

747 With the restriction $S = (D - GP)^T(D - GP)$ as a minimum, GA is introduced as an
748 optimization solution search in the model parameters space.

749 Assuming that the parameters matrix P is the population (solutions), the
750 $S = (D - GP)^T(D - GP)$ is an objective function, $l_i = \frac{1}{S}$ is the value of individual
751 fitness, and $L = \sum_{i=1}^n l_i$ is the value of total fitness. The operating steps of GA include:
752 creation and coding of initial population (solutions), fitness calculation, the choice of
753 male parents, crossover and variation, etc. A detailed theoretical explanation can be
754 got from Wang (2001). The step length is 1 month during the calculation. After
755 optimization searches and genetic operations, the target value can be rapidly
756 converged on and each optimal parameter of the dynamical equations can be obtained.

757 Through the above approach, we can obtain parameters of a nonlinear
758 dynamical system, and reconstruct the nonlinear dynamical equations from observed
759 data.

760

761 **APPENDIX B: THE MATHEMATICAL PRINCIPLE OF** 762 **SELF-MEMORIZATION DYNAMICS OF SYSTEMS**

763 The dynamical equations of a system can be expressed as:

$$764 \quad \frac{\partial x_i}{\partial t} = F_i(x, \lambda, t) \quad i = 1, 2, \dots, J \quad (\text{B1})$$

765 where J is an integer, x_i is the i th variable of the system state, and λ is
766 the parameter. Equation (B1) represents the relationship between a source function

767 F and a local change of x . Obviously, x is a scalar function with time t and
768 space r_0 . A set of time $T=[t_p\dots t_0\dots t_q]$ can be considered, where t_0 is an initial
769 time. A set of space $R=[r_a\dots r_i\dots r_\beta]$ can be considered, where r_i is a spatial point.
770 An inner product in space $L^2:T\times R$ is defined by:

$$771 \quad (f, g) = \int_a^b f(\xi)g(\xi)d\xi, f, g \in L^2 \quad (\text{B2})$$

772 Accordingly, a norm can be defined as:

$$773 \quad \|f\| = [\int_a^b (f(\xi))^2 d\xi]^{1/2}$$

774 For a completion L^2 , it can become a Hilbert space H . A generalized one
775 in H can be regarded as a solution of the multi-time model. By introducing a
776 memorization function $\beta(r, t)$, we can obtain:

$$777 \quad \int_{t_0}^t \beta(\tau) \frac{\partial x}{\partial \tau} d\tau = \int_{t_0}^t \beta(\tau) F(x, \tau) d\tau \quad (\text{B3})$$

778 where r in $\beta(r, t)$ can be dropped through fixing on the spatial point r_0 . Suppose
779 that function $\beta(r, t)$ and variable x etc. are all continuous, differentiable and
780 integrable, an integration by the left parts of Eq. (B3) can be made as:

$$781 \quad \int_{t_0}^t \beta(\tau) \frac{\partial x}{\partial \tau} d\tau = \beta(t)x(t) - \beta(t_0)x(t_0) - \int_{t_0}^t x(\tau)\beta'(\tau)d\tau \quad (\text{B4})$$

782 where $\beta'(t) = \partial\beta(t)/\partial t$. The mean value theorem can be introduced into the third
783 term in Eq. (B4), the following equation can be obtained:

$$784 \quad -\int_{t_0}^t x(\tau)\beta'(\tau)d\tau = -x^m(t_0)[\beta(t) - \beta(t_0)] \quad (\text{B5})$$

785 where $x^m(t_0) \equiv x(t_m), t_0 < t_m < t$. Substituting Eq. (B4) and Eq. (B5) in Eq. (B3) and
786 carrying out an algebraic operation, the following equation can be obtained:

787
$$x(t) = \frac{\beta(t_0)}{\beta(t)} x(t_0) + \frac{\beta(t) - \beta(t_0)}{\beta(t)} x^m(t_0) + \frac{1}{\beta(t)} \int_{t_0}^t \beta(\tau) F(x, \tau) d\tau \quad (B6)$$

788 Because the x value which is at initial time t_0 and middle time t_m , only on
 789 the fixed point r_0 itself, relates to the first term and the second term in Eq. (B6),
 790 they are called as a self-memory term. Also, we can call the third term as an
 791 exogenous effect, i.e., which is contributed by other spatial points.

792 Similarly as Eq. (B4), for multi-time $t_i, i = -p, -p+1, \dots, t_0, t$, it gives

793
$$\int_{t-p}^{t-p+1} \beta(\tau) \frac{\partial x}{\partial \tau} d\tau + \int_{t-p+1}^{t-p+2} \beta(\tau) \frac{\partial x}{\partial \tau} d\tau + \dots + \int_{t_0}^t \beta(\tau) \frac{\partial x}{\partial \tau} d\tau = \int_{t-p}^t \beta(\tau) F(x, \tau) d\tau.$$

794 After the same term $\beta(t_i)x(t_i), i = -p+1, -p+2, \dots, 0$ was eliminated, we
 795 have

796
$$\beta(t)x(t) - \beta(t_{-p})x(t_{-p}) - \sum_{i=-p}^0 [\beta(t_{i+1}) - \beta(t_i)]x^m(t_i) - \int_{t-p}^t \beta(\tau) F(x, \tau) d\tau = 0 \quad (B7)$$

797 As a matter of convenience, we set $\beta_t \equiv \beta(t), \beta_0 \equiv \beta(t_0), x_t \equiv x(t), x_0 \equiv x(t_0)$; the
 798 following text uses similar notations. Then, Eq. (B7) can be expressed as:

799
$$\beta_t x_t - \beta_{-p} x_{-p} - \sum_{i=-p}^0 x_i^m (\beta_{i+1} - \beta_i) - \int_{t-p}^t \beta(\tau) F(x, \tau) d\tau = 0 \quad (B8)$$

800 Setting $x_{-p} \equiv x_{-p-1}, \beta_{-p-1} = 0$, the Eq. (B8) can be written as:

801
$$x_t = \frac{1}{\beta_t} \sum_{i=-p-1}^0 x_i^m (\beta_{i+1} - \beta_i) + \frac{1}{\beta_t} \int_{t-p}^t \beta(\tau) F(x, \tau) d\tau = S_1 + S_2 \quad (B9)$$

802 S_1 is called as a self-memory term and S_2 is called as an exogenous effect term.

803 For the convenience of calculations, the above self-memorization equation can
 804 be discretized. The differential by difference and the summation can replace the

805 integration in Eq. (B9), and the mean of two values which are at adjoining times; i.e.,

806 $x_i^m \approx \frac{1}{2}(x_{i+1} + x_i) \equiv y_i$ can simply replace x_i^m .

807 Taking an equal time interval $\Delta t_i = t_{i+1} - t_i = 1$ and incorporating β_i and β_t ,

808 we can obtain a discretized self-memorization equation as follows:

$$809 \quad x_t = \sum_{i=-p-1}^{-1} \alpha_i y_i + \sum_{i=-p}^0 \theta_i F(x, i) \quad (\text{B10})$$

810 where F is the ~~dynamic~~dynamical kernel of the self-memorization

811 equation, $\alpha_i = \frac{(\beta_{i+1} - \beta_i)}{\beta_t}$; $\theta_i = \frac{\beta_i}{\beta_t}$.

812 Based on Eq. (B10), the above technique performed computations and the

813 forecast can be called as a self-memorization principle.

814

815

816 REFERENCES

817 Ashok K, Guan Z, Yam agata T : Impact of the Indian Ocean Dipole on the decadal relationship
818 between the Indian mon soon rainfall and ENSO, Geophys Res Let,28(23),4499-4502,2001.

819 Balmaseda M.A., Davey M.K. and Anderson D.L.T.: Decadal and seasonal dependence of ENSO
820 prediction skill,J Clim.,8, 2705–2715,1995.

821 Barnston A. G., et al.: Skill of real-time seasonal ENSO model predictions during 2002-2011,Bull.
822 Amer. Meteor.Soc.,93, 631-651,2012.

823 Belkin M. and P. Niyogi: Laplacian eigenmaps for dimensionality reduction and data
824 representation,Netural Comput.,15,1373-1391,2003.

825 Bjerknes J.: Atmsopheric telconnections from the equorail Pacific,Mon. Wea. Rev.,97,163-172, 1969.

826 ~~Burnham, K. P.; Anderson, D. R: Model Selection and Multimodel Inference (2nd ed.),
827 Springer-Verlag, 2002.~~

828 Cao H. X.: Self-memorization Equation in Atmospheric Motion,Science in China (Series B),36(7),
829 845-855,1993.

830 Chen D., S. E. Zebiak, A. J. Busalacchi and M. A. Cane: An Improved Procedure for El Niño
831 Forecasting: Implications for Predictability, *Science*, 269, 1699-1702, 1995.

832 Chen G., Shao B. M. Han Y., et al.: Modality of semiannual to multidecadal oscillations in global sea
833 surface temperature variability. *Journal of Geophysical Research*, 115, 1-14, 2010.

834 Chen X. D., Xia J., Xu Q.: Differential Hydrological Grey Model(DHGM) with self-memory function
835 and its application to flood forecasting, *Sci China Tech Sci.*, 52, 1039–1049, 2009.

836 Clarke A. J. and S. Van Gorder: Improving El Niño prediction using a space-time integration of
837 Indo-Pacific winds and equatorial Pacific upper ocean heat content, *Geophys. Res. Lett.*, 30, 1399.
838 doi:10.1029/2002GL016673, 2003.

839 Delecluse P., Davey M., Kitamura Y., Philander S., Suarez M., Bengtsson L.: TOGA review paper:
840 coupled general circulation modeling of the tropical Pacific, *J Geophys Res*, 103, 14357–14373, 1998.

841 Davey M., Huddleston M., Sperber K.R., et al.: A study of coupled model climatology and variability
842 in tropical ocean regions, *Clim. Dyn.*, 18, 403–420, 2002.

843 Dommenges and Latif: A Cautionary Note on the Interpretation of EOFs, *Journal of*
844 *Climate*, 15(2), 216–225, 2002.

845 Drosowsky W.: Statistical prediction of ENSO (Niño 3) using sub-surface temperature data, *Geophys.*
846 *Res. Lett.*, 33, L03710. doi:10.1029/2005GL024866, 2006.

847 Everitt B.S., Skrondal A.: *Cambridge Dictionary of Statistics*, Cambridge University Press, 2010.

848 Feng G. L., Cao H. X., Gao X. Q., et al.: Prediction of precipitation during summer monsoon with
849 self-memorial model, *Adv Atmos Sci.*, 18, 701–709, 2001.

850 Fraedrich K.: Estimating weather and climate predictability on attractors, *J Atmos. Sci.*, 44, 722-728,
851 1987.

852 Glantz MH, Katz RW, Nicholls N (eds): *Teleconnections linking worldwide climate anomalies*,
853 74pp, Cambridge University Press, Cambridge, UK, 1991.

854 Golbraikh A. and Tropsha A.: Beware of q^2 ! *Journal of Molecular Graphics and Modelling*, 20,
855 269–276, 2002.

856 Golbraikh A., Shen M., Xiao Z. Y., Xiao Y. D., Lee Kuo-Hsiung, Tropsha A.: Rational selection of
857 training and test sets for the development of validated QSAR models. *Journal of Computer-Aided*
858 *Molecular Design*, 17(2), 241-253, 2003.

859 Gu X. Q.: A spectral model based on atmospheric self memorization principle, *Chinese Science*

860 Bulletin,43(20),1692-1702,1998.

861 Hong M., Zhang R., Wu G. X., et al.: A Nonlinear Dynamic System Reconstruction of the Subtropical
862 High Characteristic Index based on Genetic Algorithm. Chinese Journal of Atmospheric
863 Sciences,31(2):346-352,2007.

864 Hong M., Zhang R.andMa C. C.et al.: A Non-Linear Dynamical–Statistical Model for Reconstruction
865 of the Air–Sea Element Fields in the Tropical Pacific Ocean,Atmosphere-Ocean, doi:
866 10.1080/07055900.2014.908765,2014.

867 Hong M., Zhang R., et al.: Reconstruction and forecast experiments of a statistical-dynamical model of
868 the Western Pacific subtropical high and Eastern Asian summer monsoon factors, Weather and
869 Forecasting, 30:206-216,2015

870 Hong M., Zhang R., et al.: Catastrophe and Mechanism Analyses of Multiple Equilibria in the Western
871 Pacific Subtropical High System Based on Objective Fitting of Spatial Basis Functions. Monthly
872 Weather Review, 144, 997-1015,2016.

873 Hong M., Zhang R., et al.: Bifurcations and catastrophes in a nonlinear dynamical model of the western
874 Pacific subtropical high ridge line index and its evolution mechanism, Theor. Appl. Climatol., 129,
875 363-384,2017.

876 Hu, T.S., K.C. Lam, and S.T. Ng: River flow time series prediction with a range-dependent neural
877 network,Hydrol. Sci. J., 46, 729–745,2001.

878 Hu Y. J., Zhong Z., Zhu Y. M. et al.: A statistical forecast model using the time-scale decomposition
879 technique to predict rainfall during flood period over the middle and lower reaches of the Yangtze
880 River Valley. Theoretical and Applied Climatology, doi: 10.1007/s00704-017-2094-9,2017.

881 Huang. J., Y. Yi, S. Wang, et al.: An analogue-dynamical long-range numerical weather prediction
882 system incorporating historical evolution,Quart J Roy Meteor Soc, 119(511),547-565,1993.

883 Islam M.N. Sivakumar B.: Characterization and prediction of runoff dynamics:a nonlinear dynamical
884 view. Advances in Water Resources, 25, 179-190,2002.

885 James A. Carton and Benjamin S. Giese: A Reanalysis of Ocean Climate Using Simple Ocean Data
886 Assimilation (SODA),Monthly Weather Review,136(8),2999-3011,2008.

887 Jin E. K., James L. K., Wang B., et al.: Current status of ENSO prediction skill in coupled
888 ocean-atmosphere models,Climate Dyn,31, 647-664,2008.

889 Johnson S.D., Battisit D.S. andSarachik E. S.: Empirically Derived Markov Models and Prediction of

890 Tropical Pacific Sea Surface Temperature Anomalies, *Journal of Climate*,13,3-17, 2000.

891 Kalnay E., Kanamitsu M. and Kistler R.: The NCEP/NCAR 40-year reanalysis project, *Bull. Amer.*
892 *Meteor. Soc.*,77,437-470, 1996.

893 Kathrin B üttner, Jennifer Salau, and Joachim Krieter: Temporal correlation coefficient for directed
894 networks. *Springerplus*, 5(1): 1198-1203,2016.

895 Kim Ji-Won ,Soon-II An,Sang-Yoon Jun,Hey-Jin Park,Sang-Wook Yeh.: ENSO and East Asian winter
896 monsoon relationship modulation associated with the anomalous northwest Pacific anticyclone,
897 *Climate Dynamics*, 49(4), 1157–1179,2017.

898 L'Heureux Michelle L., Collins Dan C., Hu Zeng-Zhen. Linear trends in sea surface temperature of the
899 tropical Pacific Ocean and implications for the El Niño-Southern Oscillation, *Climate Dynamics*, 40,
900 1223–1236,2013.

901 Liebmann B. and C.A. Smith: Description of a Complete (Interpolated) Outgoing Longwave Radiation
902 Dataset,*Bulletin of the American Meteorological Society*,77,1275-1277, 1996.

903 Luo, J.-J., S. Masson, S. Behera, S. Shingu, and T. Yamagata: Seasonal climate predictability in a
904 coupled OAGCM using a different approach for ensemble forecasts,*J. Climate*, 18,4474–4497,2005.

905 Mechoso C.R., Robertson A.W., Barth N., et al.: The seasonal cycle over the tropical Pacific in coupled
906 atmosphere–ocean general circulation models,*Mon Weather Rev*,123,2825–2838, 1995.

907 Molteni F., et al.: ECMWF seasonal forecast system3,*CLIVAR Exch*,43,7-9,2007.

908 Moore A. M., Zavala-Garay J. and Tang Y., et al.: Optimal forcing patterns for coupled models of
909 ENSO,*J. Climate*,19,4683-4699, 2006.

910 Neelin J.D., Latif M. and Allaart M.A.F.: Tropical air-sea interaction in general circulation
911 models,*Clim Dyn.*,7,73–104, 1992.

912 Nicosia V, Tang J, Mascolo C, Musolesi M, Russo G, Latora V: Graph metrics for temporal networks.
913 In: Holme P, Saramäki J, editors. *Temporal networks*. Berlin: Springer, pp. 15–40,2013,.

914 Palmer T. N., Alessandri A. and Andersen U., et al.: Development of a European multi-model
915 ensemble system for seasonal to interannual prediction (DEMETER),*Bull Amer Met Soc.*,85,853-872 ,
916 2004.

917 Philander S G, Pacanowski R.C., N-C Lau et al.: Simulation of ENSO with a global atmospheric GCM
918 coupled to a high resolution, tropical Pacific Ocean GCM. *J.Climate*, 5,308-329,1992.

919 Qin G. H. and Li Z. H.: Over-fitting of BP NN research and its application, *Engineering Journal of*

920 Wuhan University,39(6),1671-1679 ,2006.

921 Rasmusson E.M. and Carpenter T.H.: Variations in tropical seasurface temperature and surface wind
922 fields associated with the Southern Oscillation/E1 Niño,Mon Weather Rev.,10, 354-384,1982.

923 Rayner NA, Parker DE, Horton EB, Folland CK, Alexander LV, Rowell DP, Kent EC, Kaplan A:
924 Global analyses of sea surface temperature, sea ice, and night marine air temperature since the late
925 nineteenth century.J Geophys Res 108(D14):4407. doi:10.1029/2002JD002670, 2003.

926 Reynolds, R. W., N. A. Rayner, T. M. Smith, D. C.Stokes, and W. Wang: An improved in situand
927 satellite SST analysis for climate,J. Climate,15,1609–1625,2002.

928 Saha S., Nadiga C. and Thiaw J., et al.: The NCEP climate forecast system,Journal of
929 Climate,19 ,3483-3517 ,2006.

930 Saji N. H., Goswami B. N., V. inayachandran P. N., et al.: A dipole mode in the tropical Indian
931 Ocean,Nature, 401(6751),360-363,1999.

932 Smith T.M.: Improved extended reconstruction of SST(1854-1997).J. Climate, 17, 2466-2477,2004.

933 Takens, F.: Detecting strange attractors in fluid turbulence,Lecture Notes in
934 Mathematics,898(2),361-381 ,1981.

935 Sivakumar B, Berndtsson R, Persson M.: Monthly Runoff Prediction Using Phase -space
936 Reconstruction.Hydrological Sciences Journal, 46(3),377 -388,2001.

937 Sivakumar B., Jayawardena A.W., Fernando T.M.K.G.,: River flow forecasting: use of phase-space
938 reconstruction and artificial neural networks approaches. Journal of Hydrology, 265, 225-245,2002.

939 Timmermann A., Voss H. U. and Pasmanter R.: Empirical Dynamical System Modeling of ENSO
940 Using Nonlinear Inverse Techniques, Journal of Physical Oceanography, 31,1579-1598 ,2001.

941 Tomita, T., and T. Yasunari: Role of the northeast winter monsoon on the biennial oscillation of the
942 ENSO/monsoon system,J. Meteor. Soc. Japan, 74,399–413 ,1996.

943 Trenberth, E. K., et al.: Progress during TOGA in understanding and modeling global teleconnections
944 associated with tropical sea surface temperatures,J. Geophys. Res., 107,C7, 14291-14324,1998.

945 Wang B., Wu R., Lukas R.: Roles of western North Pacific wind variation in thermocline adjustment
946 and ENSO phase transition,J Meteor Soc Japan,77,1-16,1999a.

947 Wang B., Wu R., Li T.: Atmosphere-warm ocean interaction and its impacts on Asian-Australian
948 monsoon variation.J. Climate, 16, 1195-1211,2003.

949 Wang B., Lee J. Y., Shukla J., et al.: Advance and prospectus of seasonal prediction: assessment of

950 the APCC / CliPAS 14-Model Ensemble Retrospective Seasonal Prediction(1980—2004),Climate
951 Dyn.,33(1),93-117 ,2009a.

952 Wang C., Weisberg R. H. and Virmani J. I.: Western Pacific interannual variability associated with the
953 El Niño-Southern Oscillation,J Geophy Res.,104,5131-5149, 1999b.

954 Wang, L., W. Chen, and R. H. Huang: Interdecadal modulation of PDO on the impact of ENSO on the
955 east Asian winter monsoon, Geophys. Res. Lett., 35, L20702, doi:10.1029/2008GL035287, 2008.

956 Wang, W. C., K. W. Chau, C. T. Cheng, and L. Qiu: A comparison of performance of several artificial
957 intelligence methods for forecasting monthly discharge time series. J. Hydrol., 374, 294–306,
958 doi:10.1016/j.jhydrol.2009.06.019,2009b.

959 Wang L.: Intelligent Optimization Algorithms and Its Application, pp. 23-24, Tsinghua University
960 Press, Chendu, 2001.

961 Webster P. J., Moore A. M., Loschnigg J. P., et al.: Coupled ocean-atmosphere dynamics in the Indian
962 Ocean during 1997- 98,Nature, 401(6751),356-360, 1999.

963 Weinberger K. Q. and L. Saul: Unsupervised learning of image manifolds by semidefinite
964 programming,Int. J. Comput. Vision.,70, 77-90,2006.

965 Xu B.C., Wang Z.S., Wu J.P. and Zhou E.M.: Interaction between sea surface temperature (SST) of
966 information regions and southern oscillation index (SOI) in Tropical Pacific Ocean. *Marine Science
967 Bulletin*, 12(5),211-25,1993.

968 Yang, S., K. M. Lau, and K. M. Kim: Variations of the East Asian jet stream and
969 Asian-Pacific-American winter climate anomalies, J. Climate, 15,306–325 ,2002.

970 Yang Se-Hwan and Lu Riyu: Predictability of the East Asian winter monsoon indices by the coupled
971 models of ENSEMBLES, Advances in Atmospheric Sciences, 31(6), 1279–1292,2014

972 Yim SY, Wang B, Kwon M: Interdecadal change of the controlling mechanisms for East Asian early
973 summer rainfall variation around the mid-1990s.ClimDyn., 42,1325–1333,2013.

974 Yim, S.-Y., B. Wang, W. Xing, M.-M.Lu: Prediction of Meiyu rainfall in Taiwan by multi-lead
975 physicalempriricalmodels.Clim. Dyn., 44 (11-12), 3033-3042, doi:10.1007/s00382-014-2340-0,2015.

976 Yoon, J., and S. W. Yeh: Influence of the Pacific Decadal Oscillation on the relationship between El
977 Niño and the northeast Asian summer monsoon, J. Climate,23, 4525–4537,2010.

978 Yu H., J. Huang, and J. Chou: Improvement of Medium-Range Forecasts Using the
979 Analogue-Dynamical Method,Mon. Wea. Rev., 142, 1570–1587, doi:
53

980 <http://dx.doi.org/10.1175/MWR-D-13-00250.1>, 2014a.

981 Yu H., J. Huang, W. Li, and G. Feng: Development of the analogue-dynamical method for error
982 correction of numerical forecasts, *J. Meteor. Res.*, 28(5), 934–947, doi: 10.1007/s13351-014-4077-4 ,
983 2014b.

984 Zhang R. and Hong M., et al.: Non-linear Dynamic Model Retrieval of Subtropical High Based on
985 Empirical Orthogonal Function and Genetic Algorithm, *Applied Mathematics and
986 Mechanics*, 27(12), 1645-1654, 2006.

987 Zhang R. and Hong M., et al.: Retrieval of the non-linear dynamic forecast model of El Nino/La Nina
988 index based on the genetic algorithm optimization. *Chinese Journal of Geophysics*, 51(5), 1354-1362,
989 2008.

990 Zhang R. H., Zhou G. Q. and Chao J. P.: ENSO Dynamics and Its Prediction, *Chinese Journal of
991 Atmospheric Sciences*, 27(4) ,674-688, 2003a.

992 Zhang, R.H., S. E. Zebiak, R. Kleeman, and N. Keenlyside: A new intermediate coupled model for El
993 Niño simulation and prediction. *Geophys. Res. Lett.*, 30, doi:10.1029/2003GL018010, 2003b.

994 Zhang, R. H., A. Sumi, and M. Kimoto: Impact of El Niño on the East Asian monsoon: A diagnostic
995 study of the '86/87 and '91/92 events, *J. Meteor. Soc. Japan*, 74, 49–62, 1996.

996 Zhang Y. L., Yu Y. Q., Duan W. S.: The spring prediction barrier of ENSO in retrospective prediction
997 experiments as shown by the four coupled ocean-atmosphere models. *Acta Meteorologica Sinica*, 70(3),
998 506-519, 2012.

999 Zhao J. H., Liu X. Y. and Jiang H. Y., et al.: Characteristics of Sea Surface Height in Tropical Pacific
1000 and its relationship with ENSO events, *Meteorological and Environmental Sciences*, 35(2), 33-39,
1001 2012.

1002 Zheng C. W., Pan J., Li C. Y.. Global oceanic wind speed trends. *Ocean & Coastal Management*, 129,
1003 15-24, 2016.

1004 Zheng C. W., Wang Q., Li C. Y.. An overview of medium- to long-term predictions of global wave
1005 energy resources. *Renewable and Sustainable Energy Reviews*, 79 , 1492-1502, 2017.

1006 Zhou, L.-T., and R. G. Wu: Respective impacts of the East Asian winter monsoon and ENSO on winter
1007 rainfall in China, *J. Geophys. Res.*, 115, doi: 10.1029/2009JD012502, 2010.

1008

1009

1010
1011
1012
1013
1014
1015
1016
1017
1018
1019
1020
1021
1022
1023
1024
1025
1026
1027
1028
1029
1030
1031
1032
1033
1034
1035
1036
1037
1038
1039
1040
1041
1042
1043
1044
1045
1046

List of Figures:

1048 **Fig.1**(a, c) First and second modes of the EOF deconstruction of the SSTA field, and (b, d) the
1049 corresponding PC time series.

1050 **Fig. 2** Forecast results of the first time coefficient series (a) and the second time coefficient series (b) of
1051 the SSTA field by the original model

1052 **Fig. 3.** The cross-validated retroactive hindcast results of the first time coefficient series (a) and the
1053 second time coefficient series (b) of the SSTA field by the original model

1054 **Fig. 4.** Long-term step-by-step forecast results of the first time coefficient series (a) and the second
1055 time coefficient series (b) of the SSTA field by the improved model

1056 **Fig. 5.** The cross-validated retroactive hindcast results of the first time coefficient series (a) and the
1057 second time coefficient series (b) of the SSTA field by the improved model

1058 **Fig. 6.** The forecast SSTA field (a) and the actual SSTA field (b) of an El Niño event (Dec.1997)

1059 **Fig. 7.** The forecast SSTA field (a) and the actual SSTA field (b) of a La Niña event (Dec.1999)

1060 **Fig. 8.** The forecast SSTA field (a) and the actual SSTA field (b) of neutrals event (Nov.2002)

1061 **Fig. 9.** The improved dynamical-statistical model prediction of the ENSO index

1062 **Fig. 10.** Temporal correlation between model forecasts and observations for all seasons combined, as a
1063 function of lead time. Each line highlights one model.

1064 **Fig.11.** RMSE in standardized units, as a function of lead time for all seasons combined. Each line
1065 highlights one model.

1066

1067

1068

1069

1070

1071 **Table captions:**

1072 **Table 1.** The correlation analysis between the front two time series T_1, T_2 and nine impact factors

1073 **Table 2.** The CC and MAPE of long-term fitting test when the retrospective order p is different

1074 **Table 3.** The forecast results of T_1 and T_2 in different examples within 6 and 12 months

1075 **Table. 4.** The TC and the MAPE between model forecasts and observations within 12 months for
1076 Nov.–Jan., Dec.–Feb., and Jan.–Mar. as lead time of winter, for Feb.–Apr. , Mar.–May and Apr.–June
1077 as lead time of spring, for May-July, June-August and July-Sep. as lead time of summer and for
1078 August-Oct., Sep.-Nov. and Oct.-Dec. as lead time of autumn.

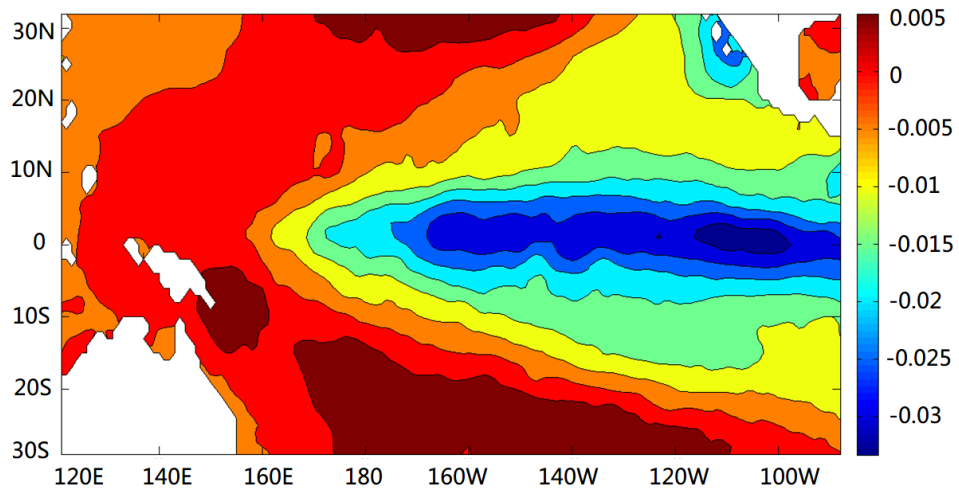
1079

1080 **Table 5.** The forecast results of the different data periods

1081

1082

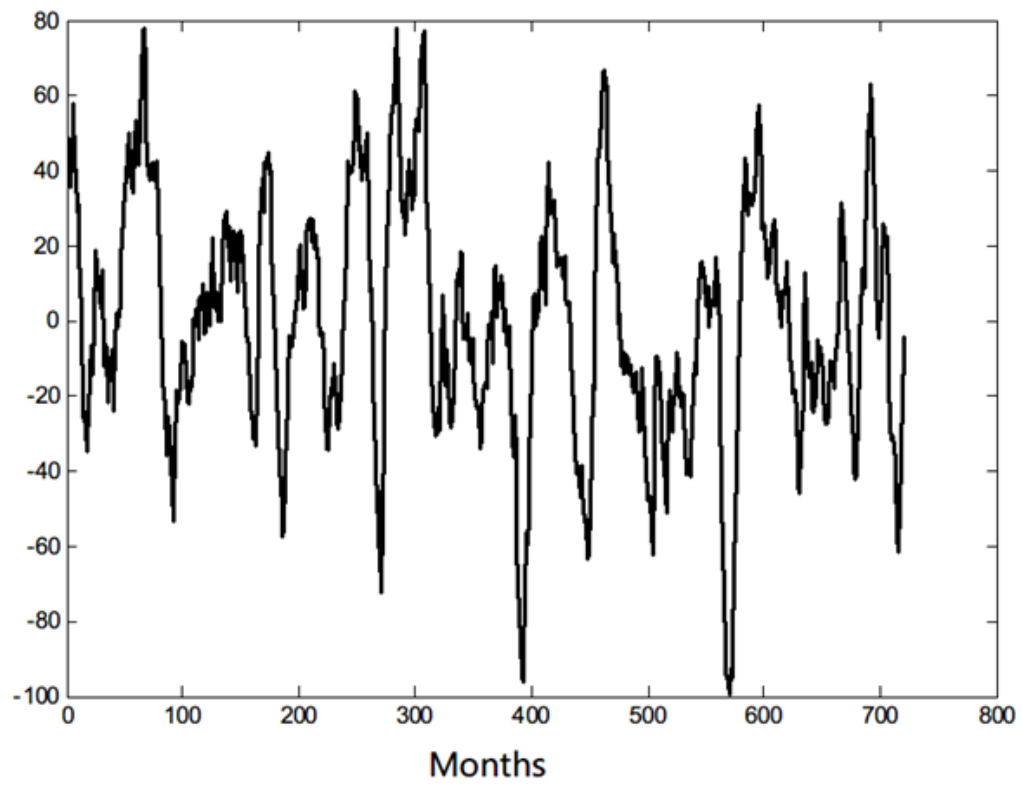
1083 **Figure:**



1084

1085

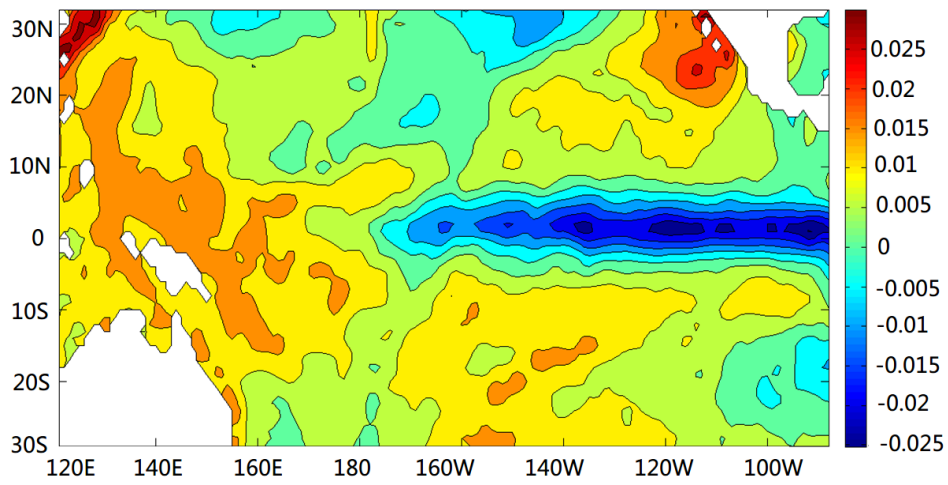
(a)



1086

1087

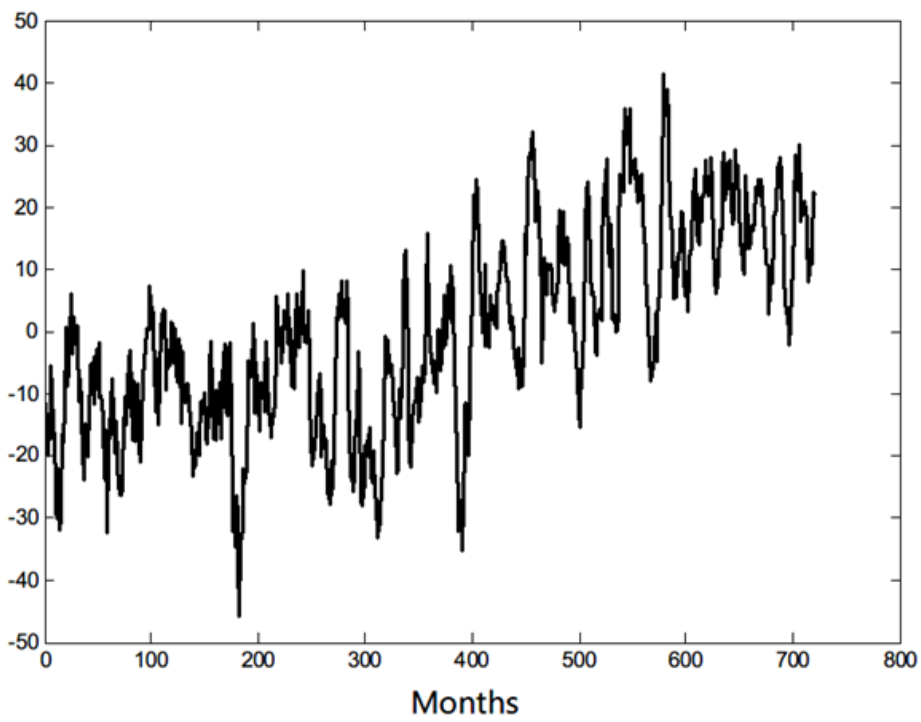
(b)



1088

1089

(c)



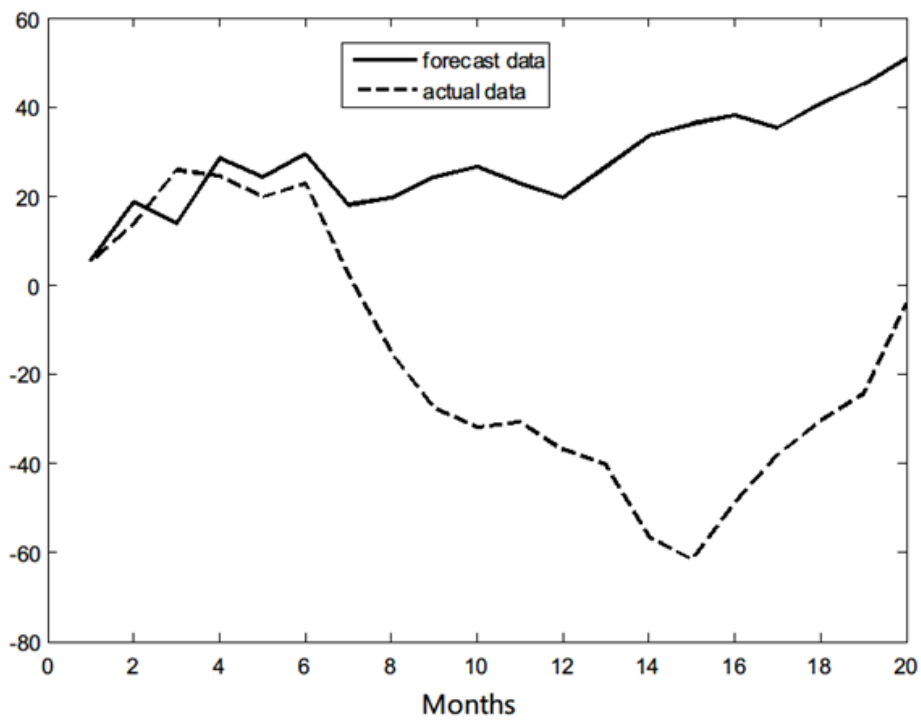
1090

1091

(d)

1092 **Fig. 1** (a, c) First and second modes of the EOF deconstruction of the SSTA field, and (b, d) the

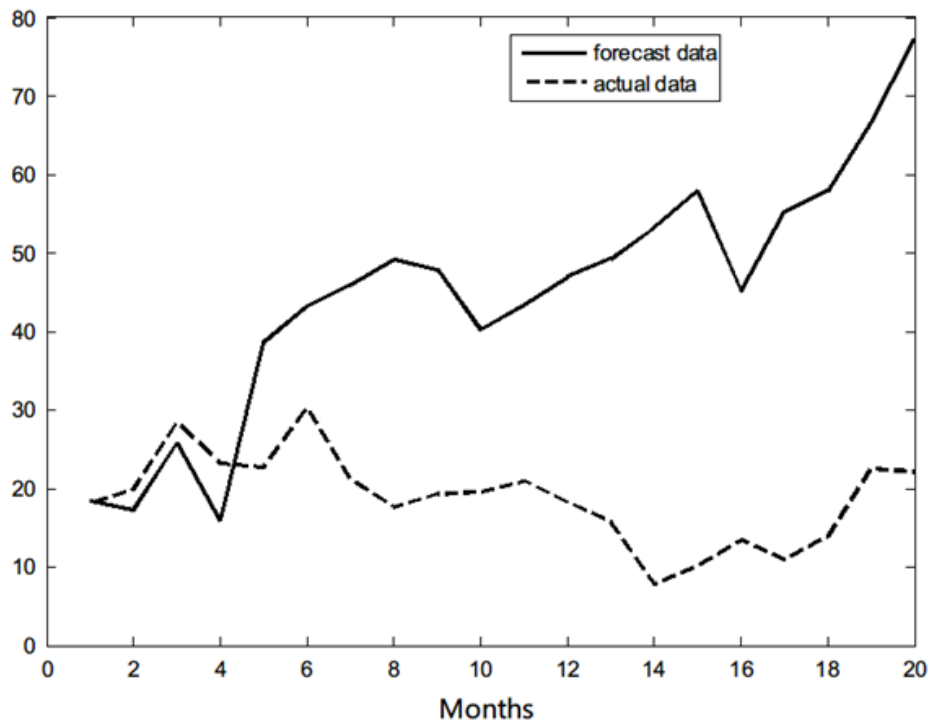
1093 corresponding PC time series.



1094

1095

(a)



1096

1097

(b)

1098 Fig.2 Forecast results of the first time coefficient series T_1 (a) and the second time coefficient series

1099 T_2 (b) of the SSTA field by the original model

1100

1101

1102

1103

1104

1105

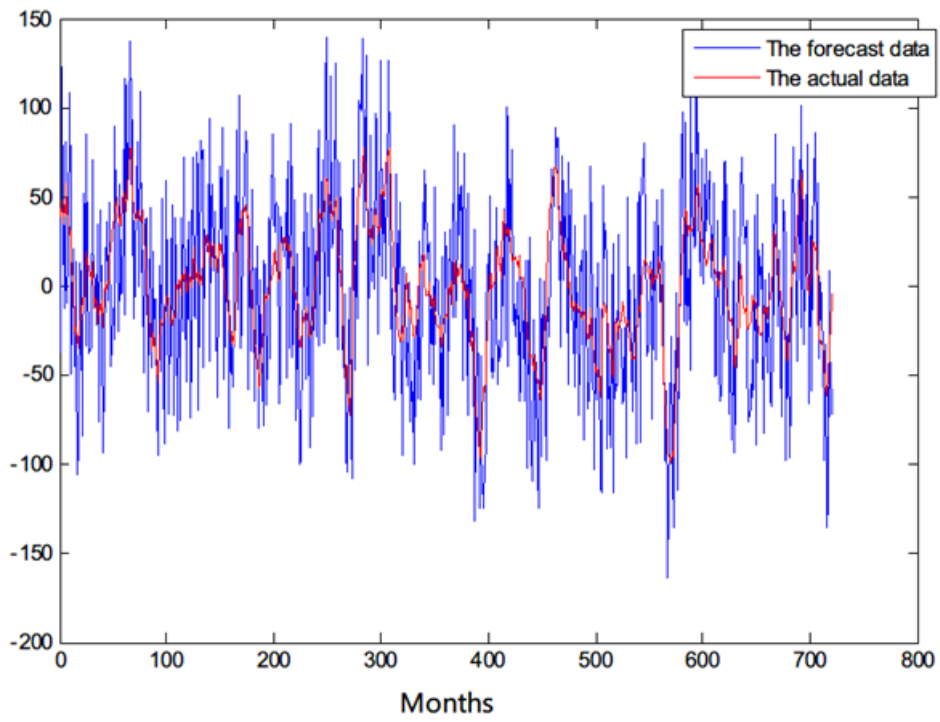
1106

1107

1108

1109

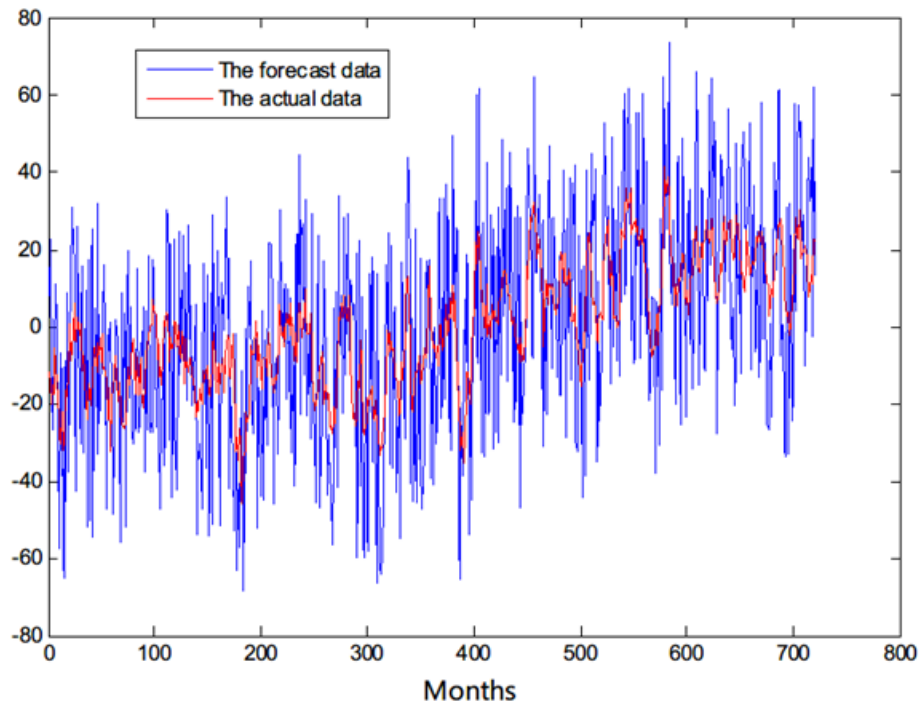
1110



1111

1112

(a)



1113

1114

(b)

1115 Fig.3 The cross-validated retroactive hindcast results of the first time coefficient series T_1 (a) and the

1116 second time coefficient series T_2 (b) of the SSTA field by the original model

1117

1118

1119

1120

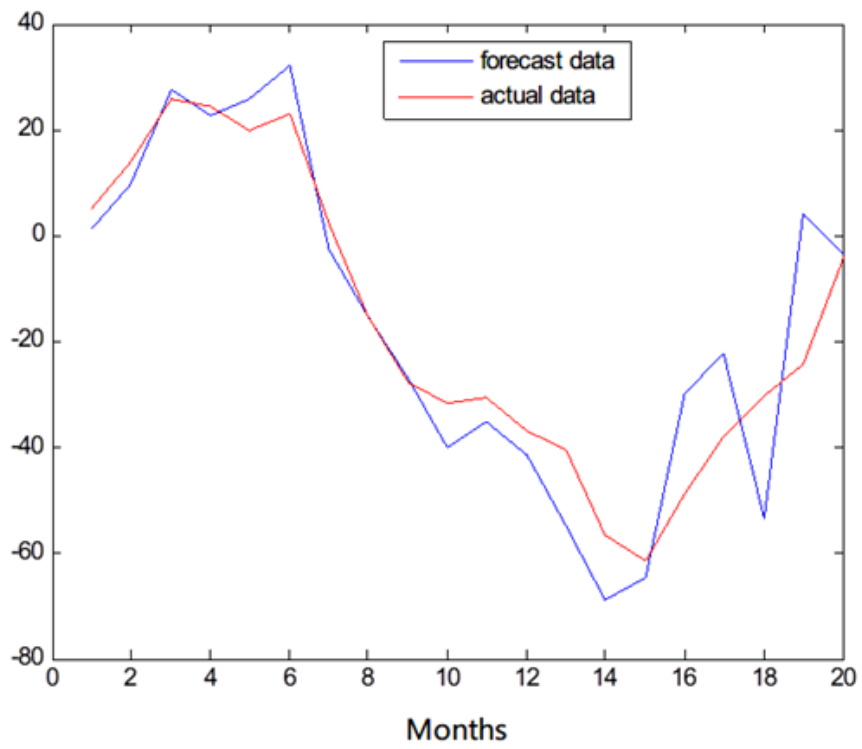
1121

1122

1123

1124

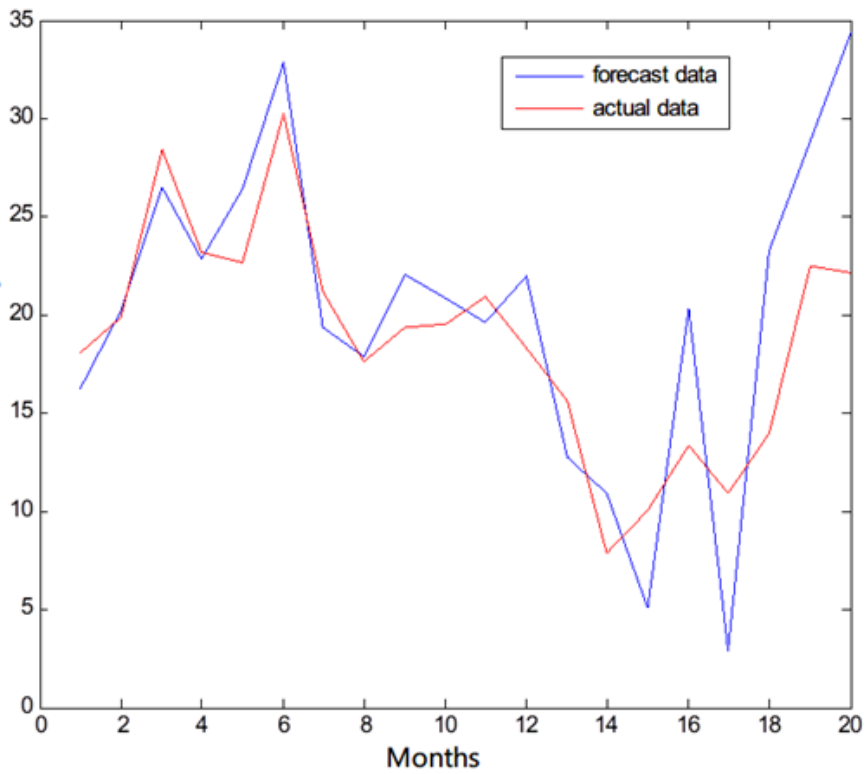
1125



1126

1127

(a)



1128

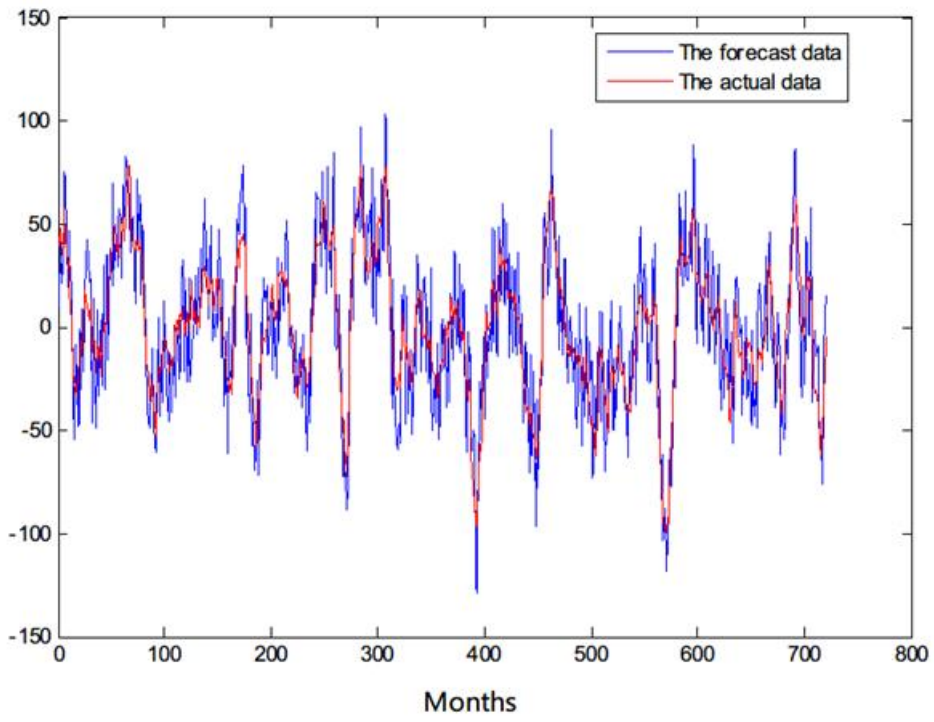
1129

(b)

1130 Fig. 4. Long-term step-by-step forecast results of the first time coefficient series T_1 (a) and the second

1131 time coefficient series T_2 (b) of the SSTA field by the improved model

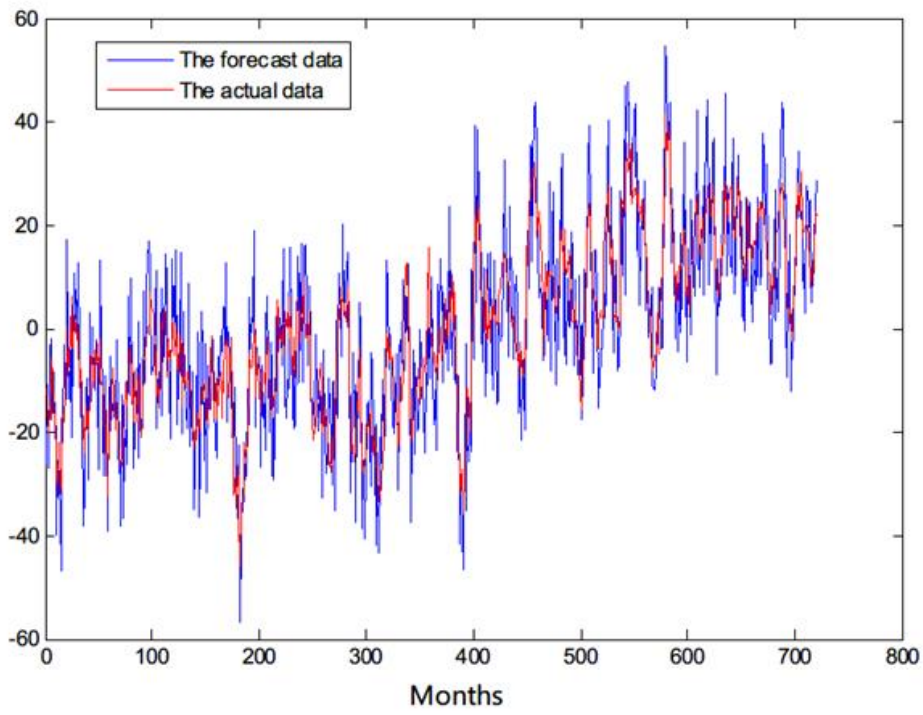
1132



1133

1134

(a)



1135

1136

(b)

1137 Fig. 5. The cross-validated retroactive hindcast results of the first time coefficient series T_1 (a) and the

1138 second time coefficient series T_2 (b) of the SSTA field by the improved model

1139

1140

1141

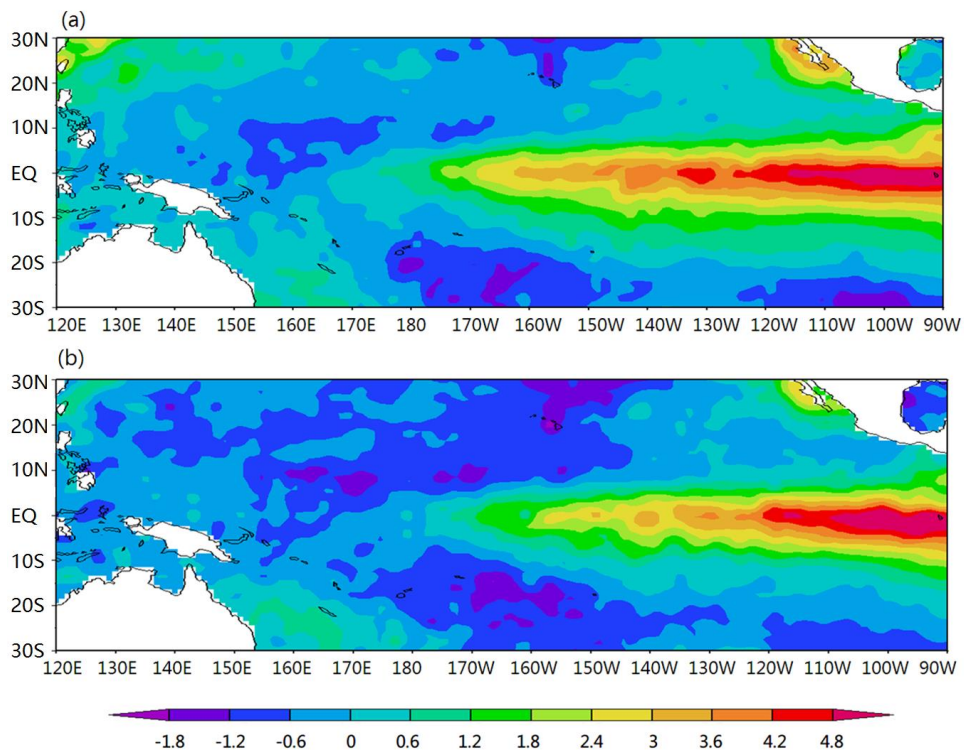
1142

1143

1144

1145

1146



1147

1148 Fig.6. The forecast SSTA field(a) and the actual SSTA field (b)of an El Niño event (Dec.1997)

1149

1150

1151

1152

1153

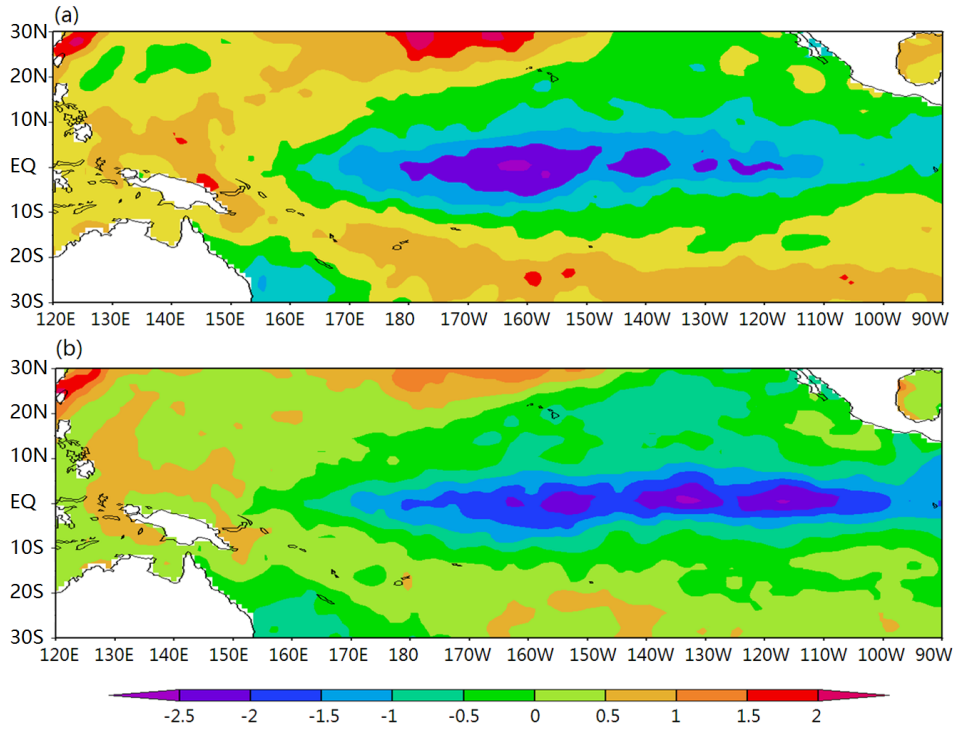
1154

1155

1156

1157

1158



1159

1160 Fig.7. The forecast SSTA field(a) and the actual SSTA field (b)of a La Niña event (Dec.1999)

1161

1162

1163

1164

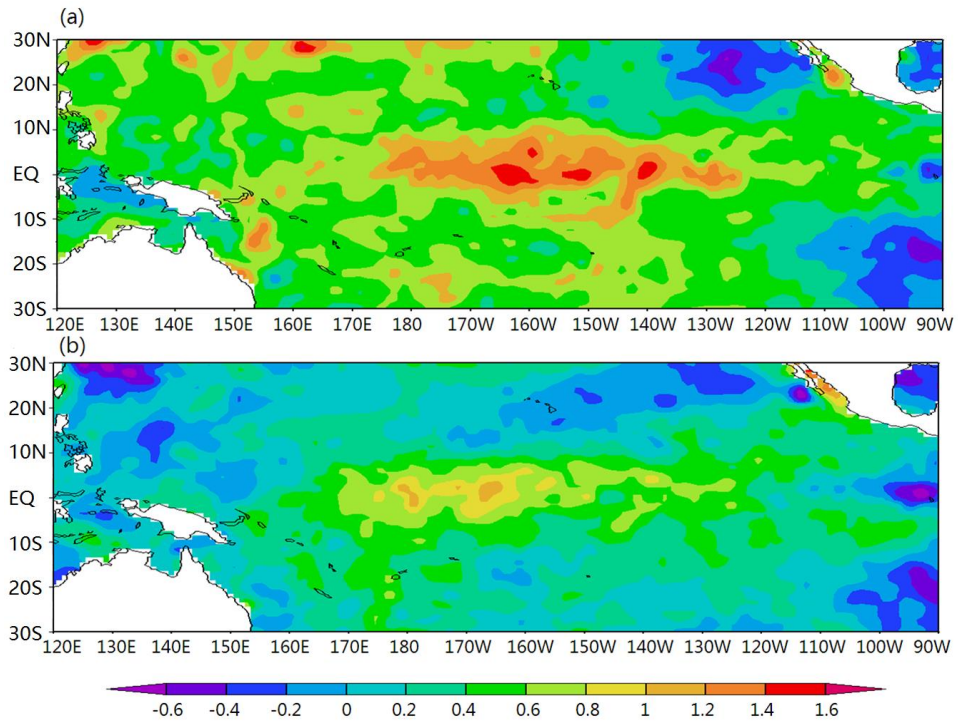
1165

1166

1167

1168

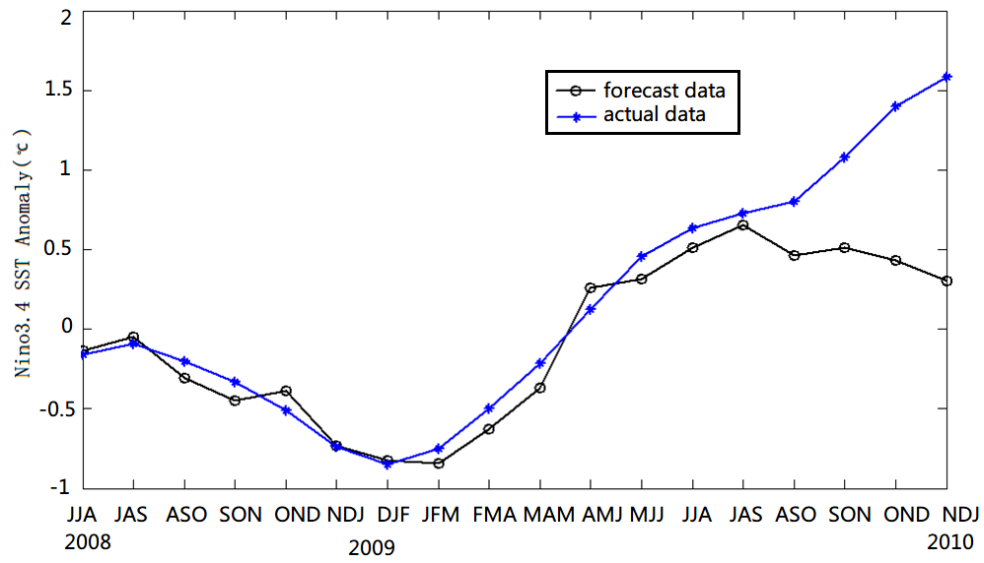
1169



1170

1171 Fig.8. The forecast SSTA field(a) and the actual SSTA field (b)of neutral event (Nov.2002)

1172



1173

1174

Fig.9. The improved dynamical-statistical model prediction of the ENSO index

1175

1176

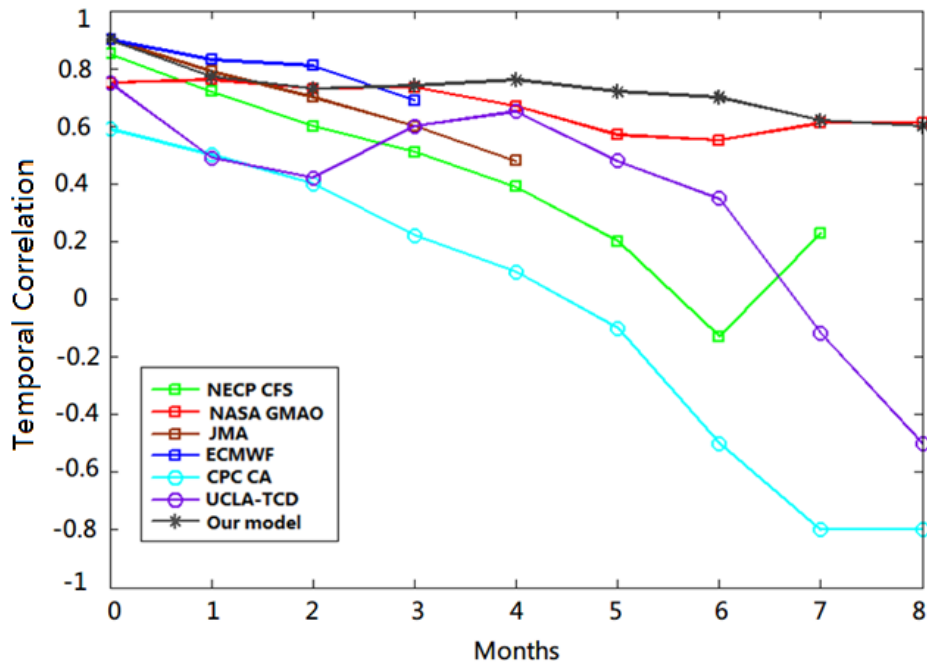
1177

1178

1179

1180

1181



1182

1183 Fig. 10. Temporal correlation between model forecasts and observations for all seasons combined, as a
 1184 function of lead time. Each line highlights one model.

1185

1186

1187

1188

1189

1190

1191

1192

1193

1194

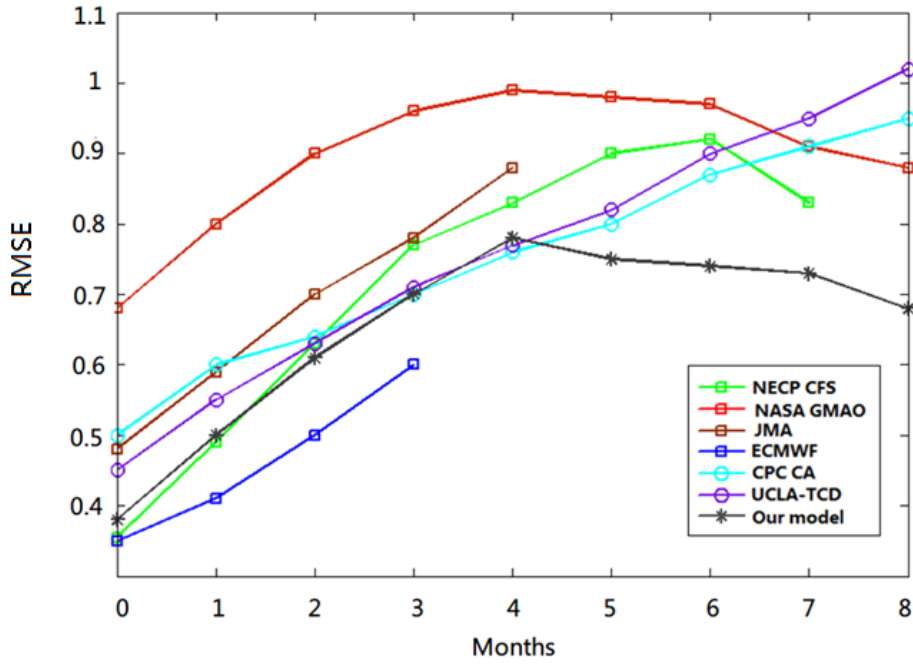
1195

1196

1197

1198

1199



1200

1201 Fig . 11. RMSE in standardized units, as a function of lead time for all seasons combined. Each line

1202 highlights one model.

1203

1204

1205

1206

1207

1208

1209

1210

1211

1212

1213

1214

1215

1216

1217 **Table:**

1218 Table 1. The correlation analysis between the front two time series T_1, T_2 and nine impact factors

factors	u_1	u_2	PNA	DMI	SOI	PDOI	EAWMI	OLR	SSH
T_1	0.3161	0.5684	0.4386	-0.3457	0.7734	0.4081	0.6284	0.3287	0.3363
T_2	0.2118	0.4181	0.2560	-0.2345	0.5232	0.3065	0.4825	0.1816	0.2169

1219

1220

1221

1222

1223

1224

1225

1226

1227

1228

1229

1230

1231

1232

1233

1234

1235

1236

1237

1238

1239

1240

1241

1242

1243

1244

1245

1246

1247

1248

1249

1250

1251

1252 **Table 2.** The CC and MAPE of long-term fitting test when the retrospective order p is different

p		4	5	6	7	8	9	10
The forecast results of long-term fitting test	CC	0.75	0.73	0.81	0.74	0.70	0.72	0.68
	MAPE	18.42%	19.36%	14.56%	20.39%	25.31%	24.18%	27.33%
p		11	12	13	14	15	16	
The forecast results of long-term fitting test	CC	0.68	0.70	0.65	0.62	0.60	0.62	
	MAPE	28.10%	26.58%	30.91%	33.14%	34.97%	33.56%	

1253

1254

1255

1256

1257

1258

1259

1260

1261

1262

1263

1264

1265

1266

1267

1268 **Table3.** The forecast results of T_1 and T_2 in different examples within 6 and 12 months

1269

Forecast events	The results within 6-months		The results within 12-months	
	CC	MAPE	CC	MAPE
The average of 18 El Niño examples of T_1	0.824	8.45%	0.719	12.67%
The average of 22 La Niña examples of T_1	0.846	7.68%	0.740	11.28%
The average of 20 Neutral examples of T_1	0.885	6.23%	0.789	9.85%
The average of total 60 examples of T_1	0.850	7.41%	0.748	10.95%
The average of 18 El Niño examples of T_2	0.811	8.79%	0.703	13.28%
The average of 22 La Niña examples of T_2	0.833	7.35%	0.731	11.96%
The average of 20 Neutral examples of T_2	0.896	6.68%	0.795	10.08%
The average of total 60 examples of T_2	0.842	7.64%	0.740	11.71%

1270

1271

1272

1273

1274

1275

1276

1277

1278

1279

1280 **Table 4.** The TC and the MAPE between model forecasts and observations within 12 months for
 1281 Nov.–Jan., Dec.–Feb., and Jan.–Mar. as lead time of winter, for Feb.–Apr. , Mar.–May and Apr.–June
 1282 as lead time of spring, for May-July, June-August and July-Sep. as lead time of summer and for
 1283 August-Oct., Sep.-Nov. and Oct.-Dec. as lead time of autumn.

Forecast events	Lead time of all seasons combined		Lead time of summer (MJJ-JJA-JAS)		Lead time of autumn (ASO-SON-OND)		Lead time of winter (NDJ-DJF-JFM)		Lead time of spring (FMA-MAM-AMJ)	
	TC	MAPE	TC	MAPE	TC	MAPE	TC	MAPE	TC	MAPE
The average of 18 El Niño examples	0.604	9.70%	0.569	10.33%	0.632	8.85%	0.677	8.02%	0.538	11.6%
The average of 22 La Niña examples	0.625	8.97%	0.581	9.82%	0.645	8.41%	0.695	7.83%	0.579	9.82%
The average of 20 Neutral examples	0.798	5.96%	0.752	6.86%	0.831	5.31%	0.844	4.60%	0.765	7.07%
The average of total 60 examples	0.712	7.62%	0.633	8.51%	0.786	6.88%	0.776	6.52%	0.653	8.03%

1284

1285

1286

1287

1288

1289

1290

1291

1292

1293

1294

Table 5. The forecast results of the different data periods

Forecast events	The data periods (Jan. 1951-Dec.2010) Lead time of all seasons combined		The data periods (Jan. 1931-Dec.2010) Lead time of all seasons combined		The data periods (Jan. 1941-Dec.2010) Lead time of all seasons combined		The data periods (Jan. 1961-Dec.2010) Lead time of all seasons combined		The data periods (Jan. 1971-Dec.2010) Lead time of all seasons combined	
	TC	MAPE	TC	MAPE	TC	MAPE	TC	MAPE	TC	MAPE
The average of 18 El Niño examples	0.60 4	9.70%	0.68 3	9.02%	0.642	9.35%	0.57 2	10.15%	0.551	10.44%
The average of 22 La Niña examples	0.62 5	8.97%	0.70 1	8.33%	0.675	8.55%	0.58 9	9.42%	0.567	9.82%
The average of 20 Neutral examples	0.79 8	5.96%	0.84 5	5.12%	0.821	5.56%	0.74 6	6.21%	0.721	6.58%
The average of	0.71	7.62%	0.77	7.14%	0.740	7.38%	0.68	7.96%	0.652	8.15%

带格式的: 行距: 2 倍行距

带格式的: 行距: 2 倍行距

带格式的: 行距: 2 倍行距

带格式的: 行距: 2 倍行距

带格式的: 行距: 2 倍行距

带格式的: 行距: 2 倍行距

~~total 60~~ 2 1 0

examples

1295

1296

1297

带格式的: 行距: 2 倍行距